

C-RAN Zero-Forcing with Imperfect CSI: Analysis and Precode&Quantize Feedback

Niv Arad, *Student Member, IEEE*, and Yair Noam, *Member, IEEE*

Abstract

Downlink joint transmission by a cluster of remote radio-heads (RRHs) is essential for enhancing throughput in future cellular networks. This method requires global channel state information (CSI) at the processing unit that designs the joint precoder. To this end, a large amount of CSI must be shared between the RRHs and that unit. This paper proposes two contributions. The first is a new upper bound on the rate loss, which implies a lower bound on the achievable rate for an RRHs-cluster employing joint zero-forcing (ZF) with incomplete CSI with single-user decoding (SUD) at the mobile stations (MSs). The second contribution, which follows insights from the bound, is a new CSI sharing scheme that drastically reduces the significant overhead associated with acquiring global CSI for joint transmission. In a nutshell, each RRH applies a local precoding matrix that creates low-dimensional effective channels that can be quantized more accurately with fewer bits, thereby reducing the overhead of sharing CSI. In addition to the CSI sharing-overhead, this scheme reduces the data rate delivered to each RRH in the cluster.

Index Terms

Broadcast channel, multiple-input multiple-output (MIMO), joint transmission (JT), cloud radio-access network (C-RAN), 5G, finite rate feedback, zero-forcing, beamforming, lower bound, Distributed MIMO.

N. Arad and Y. Noam are with the Faculty of Engineering, Bar-Ilan University, Ramat-Gan, 5290002 Israel (e-mail: nivarad44@gmail.com; yair.noam@biu.ac.il). Some of the results reported here appeared in *IEEE ICC 2018*: “Precode and quantize channel state information sharing for cloud radio access networks, pp. 1–6. . This research was supported by an Israel Ministry of Science “Kamin” grant.

I. INTRODUCTION

Joint transmission (JT) is a key for enhancing spectrum utilization in wireless communication networks. We consider downlink JT, in which adjacent RRHs form a cluster serving multiple MSs; a setup also known as distributed multiple-input multiple-output (MIMO) (D-MIMO). The idea is to transform interference between adjacent cells into useful signals. To do so, RRHs in the cluster must share both the data and CSI. Such a high level of cooperation is the main obstacle to exploiting the vast potential of JT in practice. Cloud radio access network (C-RAN) architecture facilitates the high level of D-MIMO cooperation via a centralized base-band unit (BBU) pool connected via high data-rate links, dubbed *fronthaul*, to a large number of RRHs [1]. That BBU performs all digital processing centrally, which is excellent for JT. However, JT requires ultra high-rate data sharing and high-rate, low-latency sharing of CSI between the BBU and all RRHs, which the fronthaul does not always support. This obstacle has motivated research on reducing fronthaul data-rate (see. e.g., [2, 3]) and for the introduction of a more functional RRH, dubbed smart RRH (S-RRH), that carries out some of the digital processing [4].¹

D-MIMO setups differ from one another in the type of CSI at the transmitter (CSIT). In the first type, dubbed *centralized CSIT (C-CSIT)* [5], each S-RRH sends its CSIT to the BBU. The latter thus has a single estimate of the global CSIT, from which it calculates the joint precoding matrix (JPM). Finally, the BBU feeds each S-RRHs its corresponding JPM sub-block perfectly. In another type of CSIT, dubbed *distributed CSIT (D-CSIT)* [6–8], no single entity calculates the JPM based on a single global-CSIT estimate. Instead, each S-RRH broadcasts its local CSIT to other S-RRHs (e.g., via a low-latency wireless broadcast channel), then estimates the CSIT locally, leading to a different global-CSIT estimate for each S-RRH. Finally, the S-RRH calculates its JPM from its locally known global-CSIT.

We consider a different setup in which a centralized computation unit, having global CSI, calculates the JPM. Explicitly, each S-RRH sends its CSIT to that unit, henceforth dubbed JPM

¹ We use the term S-RRH for radio units in C-RAN architectures with functional-splitting at higher-layers (see, e.g., [4]); i.e., higher than the layer in the original C-RAN concept (dubbed today Splitting 8), where the radio unit performs only radio functions of converting baseband IQ symbols into analog signals and vice versa [4]. On higher-layer splittings, the radio unit is more functional; e.g., in Splitting 7-1, 7-2, and 7-3, the radio unit carries out low-PHY functionalities, wherein Splitting 6 it performs all PHY functionalities. The BBU functionality is divided between a central unit (CU), a distribution unit (DU), and the radio unit that execute higher to lower layer functions. The DU is typically close to the radio unit.

computation unit (JPMCU), via a low-latency albeit rate-limited link as depicted in Fig. 1.² We note that we consider only CSI-quantization errors while neglecting CSI errors due to latency (outdated CSI). Upon receiving global CSIT, the JPMCU calculates the JPM. However, unlike the C-CSIT setup (where the error is only in the CSIT at the BBU), the JPMCU does not send each S-RRH its corresponding submatrices perfectly but instead sends a quantization. The proposed setup is similar to the D-CSIT in that the employed precoding matrix contains errors compared to that of the centralized design. The difference is in the error type. While in D-CSIT, the additional JPM error (compared to C-CSIT) follows from independent CSIT-errors at each S-RRH; in the proposed scheme, that error is due to the quantization of the centralized JPM.

JT under C-CSIT and D-CSIT is a well-studied topic. The single transmitter case with C-CSIT was first studied in [9], preceded by others (see, e.g. [10]), and extended to the multi-transmitter case with C-CSIT and D-CSIT in [2, 3, 6–8, 11–19]. We focus on the case where the main factor is the limited link between S-RRHs in the cluster and the JPMCU.³ Here, in addition to reducing the fronthaul data rate, we deal with another issue; namely JT with imperfect CSI.

The paper presents two contributions. The first is a new upper bound on the rate-loss, where the JPMCU sets the overall joint-ZF precoding matrix using imperfect CSI (cf. Fig. 1), compared to perfect CSI, where CSI errors are due to quantization. That upper bound yields a lower bound on the achievable rate. We assume that each S-RRH quantizes its local CSI using random vector quantization (RVQ) [20]. Similar bounds for the broadcast channel and D-MIMO with imperfect CSI appear in [9, 10] and [14–16, 21, 22], respectively, all of which consider C-CSIT. As discussed above, the proposed bound here differs from the latter bounds due to the JPM quantization, which does not exist in the C-CSIT. Furthermore, in [9, 10], the overall channel to

² Here are examples of practical C-RAN configurations where our setup (cf. Fig. 1) is suitable. The first is where enhanced radio units (as in functional splittings 7-1,7-2,7-3 and 6 cf. [4]) are connected via wireless fronthaul to a distribution unit (DU), which, with the central unit (CU), constitutes the BBU. In this case, the JPMCU is at the BBU (cf. Fig. 1), and L1 and L2 are the same link; i.e., the fronthaul, which is wireless, hence rate limited. Another scenario is in functional splittings where the DU and CU are physically separate and connected via a mid-haul link (cf. [4]), which typically has high latency that does not support JPM calculation. In this scenario, the BBU in Fig. 1 represents the CU, each S-RRH is a DU, and L1 is the mid-haul link. Then, to facilitate JT, it is sufficient to have a rate-limited L2 link between JPMCU and S-RRHs, acting as X_n [4].

³Explicitly, we assume that each S-RRH estimates the channels between it and all MSs, and we neglect that estimation error. This assumption may be reasonable if there is channel reciprocity, as in time division duplex, where the channel estimation error at the S-RRHs is negligible compared to the quantization error in sending these channels to the JPMCU.

each terminal is quantized as a haul, whereas here, in sub-blocks. This sub-block quantization induces an entirely different CSI error distribution leading to a distinct bound. Moreover, [14–16, 21, 22] consider the large system regime, whereas the analysis here does not.⁴ Finally, [16, 22] deal with channel impairment due to pilot contamination, whereas in this paper, the error is due to CSI quantization. Another relevant rate-loss bound is [6], which, unlike here, considers the D-CSIT setup, which is different as discussed above. Moreover, the bound [6] differs from the proposed bound because it assumes single-antenna transmitters and considers the high-signal-to-noise ratio (SNR) regime. A recent bound under no such assumption for the D-CSIT setup appears in [7]. However, beyond the D-CSIT, the latter bound considers the large system regime, whereas the proposed bound does not.

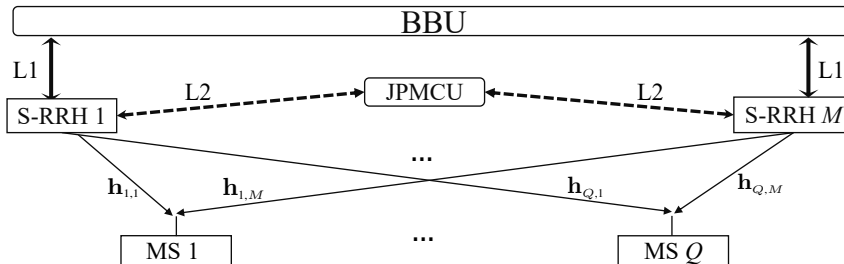


Fig. 1. System model. Link L1 interconnects the S-RRHs to higher-level C-RAN functions (see Footnote 2 for details). The joint precoding-matrix computation unit (JPMCU), located close to the S-RRHs, is connected via the low-latency, rate-limited link L2.

The second contribution is a new scheme for precoding and CSI sharing, dubbed precode and quantize (P&Q), which has two advantages. First, it reduces the number of CSI quantization bits transferred on the L2-link (cf. Fig. 1) between the S-RRHs and the JPMCU. The second advantage is that it reduces the overall fronthaul data rate between the S-RRHs and the BBU. There are different approaches for reducing JT CSI-overhead. One method, used for uplink JT, compresses the CSI delivered to the JPMCU [23]. Other techniques are robust (to inaccurate CSI) precoding [24, 25] and compressive CSI acquisition [26]. De Kerret and Gesbert [8] proposed spatial CSIT allocation policies maximizing the generalized degrees of freedom. The latter study indicates that TX cooperation should be limited to a specific finite neighborhood around each TX.

⁴The large system regime is where the number of RRH-antenna and the number of terminals grows to infinity, while their ratio approaches a nontrivial limit. In this regime, it is possible to use random matrix theory.

Sanguinetti et al. [15] designed linear precoders that minimize power consumption under a target-rate constraint and further analyzed its performance in the large system regime. Pan et al. [17] proposed a user selection algorithm and joint precoding design, which reduces implementation complexity under perfect CSIT or pilot-contamination [19]. A key distinguishing characteristic of this scheme is that it applies front-end precoding matrices at the S-RRHs before CSI quantization. These matrices aim at improving CSI accuracy at the JPCU. Each S-RRH autonomously calculates and applies a matrix, based on its local CSI, whereby creating an effective channel of lower dimensionality that can be quantized more accurately. These channels are then quantized and sent to the JPCU, which in turn calculates a joint precoding matrix and feeds it back to the S-RRHs. We show, theoretically and numerically that this scheme significantly increases the network throughput compared to the standard scheme, in which each S-RRH quantizes its local CSI and feeds it back to the JPCU. This performance gain remains for a wide range of CSI quantization bits and SNR. Equally important, the proposed feedback scheme significantly reduces the data load on the fronthaul connecting the S-RRHs and the BBU.

The organization of the paper is as follows. Sec. II introduces the system model. In Sec. III, a new upper bound on the rate-loss is presented. Sec. IV describes the P&Q CSI sharing scheme and its benefits while Sec. V analyzes its performance theoretically. Simulation results are given in Sec. VI and conclusions in Sec. VII.

Notation: Boldface lower (upper) case letters denote vectors (matrices). $(\cdot)^*$ and $(\cdot)^\dagger$ denote the conjugate and the conjugate transpose operations, respectively. Moreover, \odot and \otimes mark the Hadamard and Kronecker products, respectively. Let \mathbf{a} , be a vector, then $\bar{\mathbf{a}}$ denotes its normalized version; i.e., $\bar{\mathbf{a}} = \mathbf{a}/\|\mathbf{a}\|$. Also, $\angle\langle \mathbf{a}, \mathbf{b} \rangle$ marks the angle between \mathbf{a} and the vector \mathbf{b} . In addition, let \mathcal{Q} be a set and $q \in \mathcal{Q}$, then $\mathcal{Q}_q = \mathcal{Q} \setminus \{q\}$. Consider $\{\mathbf{A}_q\}_{q=1}^Q$, where $\mathbf{A}_q \in \mathbb{C}^{N \times M}$, then $\mathbf{A} = \text{blockdiag}(\mathbf{A}_1, \dots, \mathbf{A}_Q) \in \mathbb{C}^{QN \times QM}$ denotes the block diagonal matrix, whose q th diagonal-block is equal to \mathbf{A}_q ; i.e., $[\mathbf{A}]_{(q-1)N+n, (q-1)M+m} = [\mathbf{A}_q]_{n,m} \forall 1 \leq q \leq Q, 1 \leq n \leq N, 1 \leq m \leq M$ and is equal to zero otherwise, where $[A]_{l,m}$ denotes the (l, m) entry of \mathbf{A} . Let $\mathcal{H} = \text{span}(\mathbf{h}_1, \dots, \mathbf{h}_M)$, then $\mathbf{P}_{\mathcal{H}}, \mathbf{P}_{\mathcal{H}}^\perp$ denote the projection matrices into space spanned by \mathcal{H} and into its orthogonal complement, respectively. Also, $\chi_{\mathcal{A}}(x)$ represents the indicator function; that is, $\chi_{\mathcal{A}}(x) = 1$ if $x \in \mathcal{A}$ and 0 otherwise, \mathbf{I}_N denotes an $N \times N$ identity matrix and $\mathbf{1}_N, \mathbf{0}_N$ denote an $N \times 1$ vector of ones, and zeros, respectively. Finally, we use \log for the base 2 logarithm.

II. SYSTEM MODEL

Consider a cluster of M S-RRHs, each with N_t antennas, that jointly serve Q single-antenna MSs, as depicted in Fig. 1. We denote the set of S-RRHs $\{1, \dots, M\}$ by \mathcal{M} and the set of MSs $\{1, \dots, Q\}$ by \mathcal{Q} . Assuming flat fading channels, the *downlink* signal, observed by MS- q , is given by

$$y_q = \sum_{m=1}^M \mathbf{h}_{q,m}^\dagger \mathbf{x}_m + n_q, \quad \forall q \in \mathcal{Q} \quad (1)$$

where n_q is an additive, proper-complex Gaussian noise $n_q \sim \mathcal{CN}(0, \sigma_n^2)$, $\mathbf{x}_m \in \mathbb{C}^{N_t \times 1}$ is the signal transmitted by S-RRH- m ; $\mathbf{h}_{q,m} \in \mathbb{C}^{N_t \times 1}$ is the channel between S-RRH- m and MS- q . We further denote

$$\mathbf{h}_q \triangleq [\mathbf{h}_{q,1}^\dagger, \dots, \mathbf{h}_{q,M}^\dagger]^\dagger \in \mathbb{C}^{MN_t \times 1}. \quad (2)$$

Assumption 1: The channels are Rayleigh, independent identically distributed (i.i.d.) block-fading.⁵ Moreover, we assume large-scale fading (e.g., pathloss and shadowing effects), expressed by an attenuation factor $\alpha_{q,m}$. Explicitly, the channel $\mathbf{h}_{q,m} \sim \mathcal{CN}(\mathbf{0}_{N_t}, \alpha_{q,m} \mathbf{I}_{N_t})$, $\forall q \in \mathcal{Q}, m \in \mathcal{M}$ varies at each coherence time, whereas $\alpha_{q,m}$ remains constant during the entire codeword.

Assumption 2: We assume a practically oriented short-time power constraint P_{\max} for each S-RRH; i.e., $\mathbb{E} \{ \|\mathbf{x}_m\|^2 | U \} \leq P_{\max}$, $\forall m \in \mathcal{M}$ for every coherence-time, where U is the overall instantaneous-CSI. We further assume a linear precoding scheme in which $\mathbf{x}_m = \sum_{q \in \mathcal{Q}} s_q \mathbf{p}_{q,m}$, where $s_q \in \mathbb{C}$ is the information-bearing signal intended to MS- q and $\mathbf{p}_{q,m} \in \mathbb{C}^{N_t \times 1}$ is the precoding vector from S-RRH- m to MS- q . Finally s_1, \dots, s_q are assumed i.i.d. and $s_q \sim \mathcal{CN}(0, P_q)$.

We focus on a fully cooperative multi-cell system; thus, the joint downlink transmission can be conveniently modeled as a large multiple-input single-output (MISO) broadcast channel with MN_t transmitting antennas such that the signal observed by MS- q is

$$y_q = \mathbf{h}_q^\dagger \mathbf{p}_q s_q + \sum_{j \in \mathcal{Q}-q} \mathbf{h}_q^\dagger \mathbf{p}_j s_j + n_q, \quad \forall q \in \mathcal{Q} \quad (3)$$

⁵We use the standard definition of a block-fading channel (see [27], Ch. 5.4); that is, a channel that remains constant during a particular time block, dubbed coherence time, which is much shorter than the code block-length. This channel is drawn randomly at each coherence time and forms an ergodic sequence over time. The block-fading assumption also applies under interleaving ([27] Ch. 5.4).

where $E\{|s_q|^2\} = P_q$, $\|\mathbf{p}_q\|^2 = 1$ and \mathbf{p}_q is the overall joint beamforming vector designated for MS- q ; i.e.,

$$\mathbf{p}_q \triangleq [\mathbf{p}_{q,1}^\dagger, \dots, \mathbf{p}_{q,M}^\dagger]^\dagger \in \mathbb{C}^{MN_t \times 1}. \quad (4)$$

We assume channel reciprocity (such as in time division duplex) and consider SUD; i.e., each MS treats the interfering signals as noise. Therefore, every S-RRH estimates the channels between it and each MS served by the cluster.

Assumption 3: The long term channel characteristics are locally known at each S-RRH and globally known at the JPCMU; i.e., for each $m \in \mathcal{M}$, S-RRH- m knows $\{\alpha_{q,m}\}_{q \in \mathcal{Q}}$ whereas the JPCMU knows $\{\alpha_{q,m}\}_{m \in \mathcal{M}, q \in \mathcal{Q}}$. Since these parameters are conveyed to the JPCMU only once, we neglect the associated overhead on the L2-link (cf. Fig. 1). Moreover, for simplicity, we assume that each S-RRH- m has perfect local CSI $\{\mathbf{h}_{q,m}\}_{q \in \mathcal{Q}}$; i.e., no estimation errors.

Assumption 4: Since the L2-link is rate limited, S-RRH- m quantizes its CSI and sends the indices of the quantization codewords $\{c_{q,m}\}_{q \in \mathcal{Q}}$ with an overall number of B bits to the JPCMU. Upon receiving all the codewords $U = \{c_{q,m}\}_{q \in \mathcal{Q}, m \in \mathcal{M}}$, the JPCMU estimates \mathbf{h}_q , $\forall q \in \mathcal{Q}$ as

$$\hat{\mathbf{h}}_q \triangleq [\hat{\mathbf{h}}_{q,1}^\dagger, \dots, \hat{\mathbf{h}}_{q,M}^\dagger]^\dagger \in \mathbb{C}^{MN_t \times 1} \quad (5)$$

where $\hat{\mathbf{h}}_{q,m}$ is the estimate of $\mathbf{h}_{q,m}$, $\forall q \in \mathcal{Q}$, $m \in \mathcal{M}$.

For now, we do not restrict ourselves to a particular quantization or estimation method. Henceforth, we refer to this procedure as the *standard* CSI feedback scheme. Based on $\{\hat{\mathbf{h}}_q\}_{q \in \mathcal{Q}}$, the JPCMU calculates the overall joint precoding matrix as follows

$$\mathbf{p}_q \triangleq \mathbf{N}_q \frac{(\hat{\mathbf{h}}_q^\dagger \mathbf{N}_q)^\dagger}{\|\hat{\mathbf{h}}_q^\dagger \mathbf{N}_q\|}, \quad \forall q \in \mathcal{Q} \quad (6)$$

where the columns of $\mathbf{N}_q \in \mathbb{C}^{MN_t \times MN_t - (Q-1)}$ form an orthonormal basis for the null space of $\{\hat{\mathbf{h}}_j\}_{j \in \mathcal{Q}-q}$. Henceforth, we refer to this scheme as ZF beamforming. After setting $\mathbf{p}_q, \forall q \in \mathcal{Q}$, the JPCMU quantizes it and feeds each S-RRH with its corresponding components.

Assumption 5: For each m , the JPCMU quantizes $\{\mathbf{p}_{q,m}\}_{q \in \mathcal{Q}}$ with overall B bits and then sends to S-RRH- m . The corresponding estimate at S-RRH- m , is denoted by $\{\hat{\mathbf{p}}_{q,m}\}_{q \in \mathcal{Q}}$. Because \mathbf{p}_q is orthogonal to $\{\hat{\mathbf{h}}_j\}_{j \in \mathcal{Q}-q}$ rather than $\{\mathbf{h}_j\}_{j \in \mathcal{Q}-q}$, there is a performance loss compared to the case of perfect CSI due to residual interference, even if $\hat{\mathbf{p}}_{q,m}$ is quantized without errors. For simplicity and analytical tractability, we assume that the data signals $s_q, q \in \mathcal{Q}$ are delivered to the S-RRHs without errors.

III. DOWNLINK CRAN-JT: PERFORMANCE ANALYSIS FOR ZF WITH IMPERFECT CSI

This section introduces a new upper bound on the throughput degradation under limited CSI compared to perfect CSI. For simplicity and analytical tractability, we assume that the channel magnitude information (CMI) $\|\mathbf{h}_{q,m}\|$, $\forall q \in \mathcal{Q}$, $m \in \mathcal{M}$ is perfectly conveyed to the JPMCU. Moreover, the channel directional information (CDI) $\bar{\mathbf{h}}_{q,m} \triangleq \mathbf{h}_{q,m}/\|\mathbf{h}_{q,m}\|$ is quantized separately using RVQ [20],⁶ with independent codebooks for every q, m . We assume the same about $\{\mathbf{p}_{q,m}\}_{q \in \mathcal{Q}, m \in \mathcal{M}}$. We now review some of the properties of RVQ. Let $\hat{\mathbf{h}}_{q,m}$ be the output of RVQ with b bits. Then,

$$\bar{\mathbf{h}}_{q,m} = \sqrt{1 - Z_{q,m}} \hat{\mathbf{h}}_{q,m} + \sqrt{Z_{q,m}} \mathbf{s}_{q,m} \quad (7)$$

where $\mathbf{s}_{q,m}$ is a random vector uniformly distributed on the unit sphere of the null space of $\hat{\mathbf{h}}_{q,m}$, and $Z_{q,m}$ is a random variable, independent of $\mathbf{s}_{q,m}$, and distributed as the minimum of 2^b beta $(N_t - 1, 1)$ random variables [9]. Under the assumption of perfect CMI, the JPMCU use

$$\hat{\mathbf{h}}_{q,m} = \|\mathbf{h}_{q,m}\| \hat{\bar{\mathbf{h}}}_{q,m}, \quad (8)$$

as the estimate of $\mathbf{h}_{q,m}$.⁷ For analytical simplicity, we make the following assumption.

Assumption 6: Each S-RRH transmits equal power to every MS; i.e., $P_q = P_{q,m} = P, \forall q \in \mathcal{Q}$, $m \in \mathcal{M}$ (cf. Assumption 2 for P_q).⁸ To prevent S-RRHs from violating their power constraint P_{\max} , we set $P = \frac{P_{\max}}{Q}$. Moreover, $n_q \sim \mathcal{CN}(0, 1)$ (cf. (3)).

From (3) and Assumption 6, the signal-to-interference-plus-noise ratio (SINR) at MS- q is

$$\text{SINR}_q(\{\hat{\mathbf{p}}_i\}_{i \in \mathcal{Q}}) \triangleq \frac{P |\mathbf{h}_q^\dagger \hat{\mathbf{p}}_q|^2}{1 + P \sum_{j \in \mathcal{Q}-q} |\mathbf{h}_q^\dagger \hat{\mathbf{p}}_j|^2}, \quad \forall q \in \mathcal{Q} \quad (9)$$

where $\hat{\mathbf{p}}_q \triangleq [\hat{\mathbf{p}}_{q,1}^\dagger, \dots, \hat{\mathbf{p}}_{q,M}^\dagger]^\dagger \in \mathbb{C}^{MN_t \times 1}$, and $\hat{\mathbf{p}}_{q,m}$ is the estimate of $\mathbf{p}_{q,m}$ under RVQ, similar to (8). Assuming a Gaussian codebook and SUD, the achievable ergodic rate of MS- q with imperfect CSI is

$$\hat{R}_q \triangleq \mathbb{E} \left\{ \log \left(1 + \text{SINR}_q(\{\hat{\mathbf{p}}_i\}_{i \in \mathcal{Q}}) \right) \right\} \quad (10)$$

⁶In RVQ, the codebook is generated randomly from a uniform distribution over the unit sphere.

⁷Note that $\mathbb{E}\{\mathbf{h}_{q,m} | \|\mathbf{h}_{q,m}\|, \hat{\bar{\mathbf{h}}}_{q,m}\}$, the minimum mean square error estimate of $\mathbf{h}_{q,m}$, is given by $\mathbb{E}\{\sqrt{1 - Z_{q,m}}\} \|\mathbf{h}_{q,m}\| \hat{\bar{\mathbf{h}}}_{q,m}$. Since this paper considers only ZF-type strategies, the factor $\mathbb{E}\{\sqrt{1 - Z_{q,m}}\}$ does not affect the beamformer, and therefore, is omitted.

⁸Note that the equal power assumption is not optimal (see, e.g. [28]) and is made to simplify the analysis, which is already very complicated.

The expectation is with respect to the joint distribution of the channel and the RVQ's random codebook.⁹ To evaluate performance, later we will compare \hat{R}_q to the corresponding throughput R_q^* without quantization error; i.e.,

$$R_q^* \triangleq \mathbb{E}\{\log(1 + \text{SINR}_q(\{\mathbf{p}_i^*\}_{i \in \mathcal{Q}}))\} \quad (11)$$

where \mathbf{p}_q^* is given in (6) while substituting $\hat{\mathbf{h}}_q = \mathbf{h}_q, \forall q \in \mathcal{Q}$, and is assumed to be fed-back perfectly.

Theorem 1: Consider Assumptions 1 and 3 to 6 and define the rate loss as

$$\Delta R_q \triangleq R_q^* - \hat{R}_q \quad (12)$$

where \hat{R}_q and R_q^* are defined in (10) and (11), respectively. Consider some $q \in \mathcal{Q}$ and assume that $\mathbf{h}_{q',m}, \mathbf{p}_{q',m}$ are quantized with $B/Q \in \mathbb{N}$ bits (cf. Assumptions 4 and 5), each, $\forall q' \in \mathcal{Q}, \forall m \in \mathcal{M}$; then

$$\Delta R_q \leq \Delta \bar{R}_{1,q} + \Delta \bar{R}_{2,q} \quad (13)$$

where

$$\begin{aligned} \Delta \bar{R}_{1,q} \triangleq & \log \left\{ 1 + \frac{\alpha_q P N_t (Q-1)}{M} \times \left[\frac{1}{N_t - 1} 2^{\frac{-B}{Q(N_t-1)}} \left(2(1 - \mathcal{U}(2^{B/Q}, a)) + 2^{\frac{-B}{Q(N_t-1)}} \right) \right. \right. \\ & \left. \left. + (1 - \mathcal{U}(2^{B/Q}, a))^2 - (1 - \mathcal{U}(2^{B/Q}, a)/2 - \mathcal{U}(2^{B/Q}, 2a))^4 \right] \right\} \end{aligned} \quad (14)$$

$$\begin{aligned} \Delta \bar{R}_{2,q} \triangleq & 6R_q^* (\mathcal{U}(2^{B/Q}, a) + \mathcal{V}_M(2^{B/Q}, a)) \\ & + \frac{\pi \alpha_q P N_t}{\sqrt{\alpha_q P N_t + 1}} (\mathcal{U}(2^{B/Q}, a/2) + \mathcal{V}_M(2^{B/Q}, a/2)) \end{aligned} \quad (15)$$

Here $\alpha_q \triangleq \sum_{m=1}^M \alpha_{q,m}$, $a = \frac{1}{N_t - 1}$ and¹⁰

$$\mathcal{U}(x, a) = x\beta(x, 1+a) \quad (16)$$

$$\mathcal{V}_M(x, a) = \frac{(M-1)}{\sqrt{2M-1}} \sqrt{\mathcal{U}(x, 2a) - \mathcal{U}(x, a)^2} \quad (17)$$

where $\beta(\cdot)$ is the Beta function.

Remark 1: Under Assumption 1, the perfect-CSI rate, R_q^* , can be calculated based on known results. For example, consider the case where the long-term channel-attenuation is equal for each

⁹Note that \mathbf{p}_i is a function of the quantization $\hat{\mathbf{h}}_q$, which, in the case of RVQ, is a function of the channels $\{\mathbf{h}_{q,m}\}_{m \in \mathcal{M}}$ and of the codebook generated for each channel. Moreover, $\hat{\mathbf{p}}_i$ is a function of $\{\mathbf{p}_{i,m}\}_{m \in \mathcal{M}}$.

¹⁰Note that $\mathbb{E}\{Z_{q,m}^i\} = \mathcal{U}(2^{B/Q}, ai)$, where $Z_{q,m}$ is defined in (7).

S-RRH; i.e., $\alpha_{q,m} = \alpha_{q,m'} \forall m, m' \in \mathcal{M}$, and without loss of generality, assume that $\alpha_{q,m} = 1/M \forall m \in \mathcal{M}$. In this case, it is straightforward to show that

$$R_q^* = R^* = \mathbb{E}\{\log(1 + P|\mathbf{h}_q^\dagger \mathbf{p}_q^*|^2)\} = (\log e) e^{\frac{M}{P}} \sum_{k=0}^{T-1} \Gamma\left(-k, \frac{M}{P}\right) \left(\frac{M}{P}\right)^k \triangleq \varphi(T, P/M) \quad (18)$$

where, $T = MN_t - (Q - 1)$ and $\Gamma(\cdot, \cdot)$ is the incomplete Gamma function. In the case where $\exists m \neq m'$ such that $\alpha_{q,m} \neq \alpha_{q,m'}$, an expression for R_q^* is complicated. A closed-form expression can be found in [29] (after straightforward adaptations to ZF) in the two-user case. For more than two users, such an expression is too complicated; nevertheless, it can be approximated, see [30] Sec. IV.A for the two-user case and [31, 32] for more than two users.

Proof of Theorem 1: By the assumptions of Theorem 1 and using (9), (10), (11), and (12), it follows that

$$\begin{aligned} \Delta R_q = & \mathbb{E}\{\log(1 + P|\mathbf{h}_q^\dagger \mathbf{p}_q^*|^2)\} - \mathbb{E}\left\{\log\left(1 + P|\mathbf{h}_q^\dagger \hat{\mathbf{p}}_q|^2 + P \sum_{j \in \mathcal{Q}_q} |\mathbf{h}_q^\dagger \hat{\mathbf{p}}_j|^2\right)\right\} \\ & + \mathbb{E}\left\{\log\left(1 + P \sum_{j \in \mathcal{Q}_q} |\mathbf{h}_q^\dagger \hat{\mathbf{p}}_j|^2\right)\right\} \leq A_1 - A_2 + A_3 \end{aligned} \quad (19)$$

where $\hat{\mathbf{p}}_q$ and \mathbf{p}_q^* are defined in (9) and (11), respectively, and $A_1 = \mathbb{E}\{\log(1 + P|\mathbf{h}_q^\dagger \mathbf{p}_q^*|^2)\}$, $A_2 = \mathbb{E}\{\log(1 + P|\mathbf{h}_q^\dagger \hat{\mathbf{p}}_q|^2)\}$, $A_3 = \mathbb{E}\{\log(1 + P \sum_{j \in \mathcal{Q}_q} |\mathbf{h}_q^\dagger \hat{\mathbf{p}}_j|^2)\}$. The inequality (19) follows because $P \sum_{j \in \mathcal{Q}_q} |\mathbf{h}_q^\dagger \hat{\mathbf{p}}_j|^2 \geq 0$ and $\log(1 + x)$ is a monotone increasing function. The desired result (13) then follows from the following lemmas.

Lemma 2: Under the assumptions of Theorem 1, $A_3 \leq \Delta \bar{R}_{1,q}$ (cf. (19), (14)).

Proof: See Appendix A. ■

Lemma 3: Under the assumptions of Theorem 1, $A_1 - A_2 \leq \Delta \bar{R}_{2,q}$ (cf. (19), (15)).

Proof: See Appendix B. ■

Substituting Lemmas 2 and 3 into (19) establishes (13). ■

The following corollary simplifies the rate-gap bound in Theorem 1 as the number of quantization bits gets large.

Corollary 4: The bound $\Delta R_q \leq \Delta \bar{R}_{1,q} + \Delta \bar{R}_{2,q}$ in (13) can be further approximated as

$$\Delta \bar{R}_{1,q} + \Delta \bar{R}_{2,q} = 2^{\frac{-B}{2Q(N_t-1)}} \frac{\pi \alpha_q P N_t}{\sqrt{\alpha_q P N_t + 1}} \left[V_M\left(\frac{a}{2}\right) + \Gamma\left(\frac{a}{2} + 1\right) \right] + O\left(2^{\frac{-B}{2Q(N_t-1)}}\right) \quad (20)$$

where $\Gamma(\cdot)$ is the Gamma function and $V_M(a) = \sqrt{\Gamma(2a + 1) - \Gamma(a + 1)^2} (M - 1) / \sqrt{2M - 1}$.

Proof: Let $z = 2^{B/Q}$ and denote

$$\Delta\bar{R}_{1,q}(z) + \Delta\bar{R}_{2,q}(z) = \log(1 + W_1(z) + W_2(z)) + W_3(z) \quad (21)$$

where $\Delta\bar{R}_{1,q}$ and $\Delta\bar{R}_{2,q}$ are defined in (14) and (15), respectively, and $W_1(z) = \alpha_q P(Q-1)z^{-a}N_t(2(1 - \mathcal{U}(z, a)) + z^{-a})/M(N_t - 1)$, $W_2(z) = \alpha_q P(Q-1)N_t/M[(1 - \mathcal{U}(z, a))^2 - (1 - \mathcal{U}(z, a)/2 - \mathcal{U}(z, 2a))^4]$, $W_3(z) = \frac{\pi\alpha_q P N_t}{\sqrt{\alpha_q P N_t + 1}}[\mathcal{U}(z, a/2) + \mathcal{V}_M(z, a/2)] + 6R_q^*[\mathcal{U}(z, a) + \mathcal{V}_M(z, a)]$. It can be shown that

$$\mathcal{U}(z, a) = \Gamma(a+1)z^{-a} + O(z^{-a-\frac{1}{2}}). \quad (22)$$

By substituting the latter into $W_1(z)$, it can be shown that $W_1(z) = \frac{2\alpha_q P(Q-1)z^{-a}N_t}{M(N_t-1)} + O(z^{-2a})$. Now to $W_2(z)$. Substituting, (22), it can be shown that $W_2(z) = \alpha_q P(Q-1)N_t/M[(1 - \Gamma(a+1)z^{-a})^2 - (1 - \Gamma(a+1)z^{-a}/2)^4]$. Moreover, because $(1-x)^2 - (1-x/2)^4 = -\frac{x^4}{16} + \frac{x^3}{2} - \frac{x^2}{2}$, it follows that $W_2(z) = O(z^{-2a})$. Finally, we turn to $W_3(z)$. Because $\mathcal{U}(z, a) + \mathcal{V}_M(z, a) = (V_M(z, a) + \Gamma(a+1))z^{-a} + O(z^{-a-1})$, it follows that $W_3(z) = \frac{\pi\alpha_q P N_t}{\sqrt{\alpha_q P N_t + 1}}z^{-\frac{a}{2}} \times [V_M(a/2) + \Gamma(1+a/2)] + 6R_q^*z^{-a}[V_M(a) + \Gamma(a+1)] + O(z^{-1-\frac{a}{2}})$. Then, by substituting W_1 , W_2 and W_3 into (21) while taking lower order terms, the desired result follows. ■

We conclude this section with some insights. From Corollary 4, it follows that the rate-gap decreases at the rate $2^{\frac{-B}{2Q(N_t-1)}}$ as B increases. Furthermore, note that $\frac{\pi\alpha_q P N_t}{2\sqrt{\alpha_q P N_t + 1}} = O(\sqrt{P})$ as $P \rightarrow \infty$. Therefore, to maintain the overall number of degrees of freedom, $2^{\frac{-B}{2Q(N_t-1)}}$ should decrease at least like \sqrt{P} ; i.e., the number of bits per channel should, at least, increase linearly with the SNR in dB as well as with the number of MSs. Otherwise, the network is interference limited. This result is consistent with previous findings on the single-Tx broadcast channel (cf. [9]). Finally, the rate gap decrease $2^{\frac{-B}{2Q(N_t-1)}}$ implies that it is possible to reduce the rate gap without increasing B by having a smaller Q , or having an effective number of antennas less than N_t . The latter insight is the motivation for the P&Q CSI sharing scheme presented in the following section.

However, while ΔR_q is improved if N_t or Q decreases, R_q^* deteriorates due to a loss in antenna gain. This trade-off determines if the achievable rate, \hat{R}_q (cf. (12)), increases or decreases. In the sequel, we show that \hat{R}_q can be drastically improved under a good precoding strategy in most cases. Numerical results for the proposed bounds are given in Sec. VI.

IV. THE PRECODE AND QUANTIZE CSI SHARING SCHEME

The P&Q CSI sharing scheme aims to reduce CSI overhead in the L2-link and the fronthaul information rate. Each S-RRH, say S-RRH- m , applies a front-end precoding matrix $\mathbf{A}_m \in \mathbb{C}^{N_t \times \tilde{N}_t}$, calculated according to its local CSI $\{\mathbf{h}_{q,m}\}_{q \in \mathcal{Q}}$. This creates effective low-dimensional channels $\tilde{\mathbf{h}}_{q,m}^\dagger = \mathbf{h}_{q,m}^\dagger \mathbf{A}_m \in \mathbb{C}^{1 \times \tilde{N}_t}$, $\forall q \in \mathcal{Q}$, with $\tilde{N}_t < N_t$, that can be quantized more accurately than $\mathbf{h}_{q,m}$ [33]. We further denote the overall effective channel as $\tilde{\mathbf{h}}_q \triangleq [\tilde{\mathbf{h}}_{q,1}^\dagger, \dots, \tilde{\mathbf{h}}_{q,M}^\dagger]^\dagger \in \mathbb{C}^{M\tilde{N}_t \times 1}$.

Definition 1 (MS allocation policy): To determine \mathbf{A}_m , S-RRH- m picks a subset of the MSs $\bar{\mathcal{S}}_m \subset \mathcal{Q}$, where $|\bar{\mathcal{S}}_m| = \bar{Q}$, according to the policy detailed next. Knowing $\{\alpha_{q,m}\}_{q \in \mathcal{Q}}$ S-RRH- m , picks \bar{Q} MSs that have the most significant attenuation; that is, $\bar{\mathcal{S}}_m$ includes MSs such that $\alpha_{q,m} \leq \alpha_{q',m}, \forall q \in \bar{\mathcal{S}}_m, q' \in \mathcal{Q} \setminus \bar{\mathcal{S}}_m$.

Given $\bar{\mathcal{S}}_m$, \mathbf{A}_m is set as the projection matrix into the null space of the matrix whose columns are given by $\{\mathbf{h}_{q,m}\}_{q \in \bar{\mathcal{S}}_m}$; i.e.,

$$\mathbf{A}_m = [\mathbf{u}_1 \cdots \mathbf{u}_{\tilde{N}_t}], \quad \mathbf{u}_i \in \mathbb{C}^{N_t \times 1} \quad (23)$$

where $\tilde{N}_t = N_t - \bar{Q}$ and $\{\mathbf{u}_i\}_{i=1}^{\tilde{N}_t}$ is an orthonormal basis for the orthogonal complement of $\text{span}(\{\mathbf{h}_{q,m}\}_{q \in \bar{\mathcal{S}}_m})$. Thus, S-RRH- m now serves only $Q - \bar{Q}$ MSs, denoted by $\mathcal{S}_m = \mathcal{Q} \setminus \bar{\mathcal{S}}_m \subset \mathcal{Q}$.¹¹ From (23), and because each S-RRH has perfect local CSI, $\tilde{\mathbf{h}}_{q,m} = \mathbf{0}_{\tilde{N}_t}, \forall q \in \bar{\mathcal{S}}_m$. Thus, S-RRH- m now sends the JPCMU only $Q - \bar{Q}$ channels $\{\tilde{\mathbf{h}}_{q,m}\}_{q \in \mathcal{S}_m}$, of lower dimension $\tilde{N}_t < N_t$, which can be quantized more accurately. Denote the estimate of $\tilde{\mathbf{h}}_{q,m}$ at the JPCMU by $\hat{\mathbf{h}}_{q,m}$ and

$$\hat{\mathbf{h}}_q \triangleq [\hat{\mathbf{h}}_{q,1}^\dagger, \dots, \hat{\mathbf{h}}_{q,M}^\dagger]^\dagger \in \mathbb{C}^{M\tilde{N}_t \times 1}. \quad (24)$$

Since the JPCMU knows $\bar{\mathcal{S}}_m$ ¹² it also knows that $\tilde{\mathbf{h}}_{q,m} = \mathbf{0}_{\tilde{N}_t}, \forall q \in \bar{\mathcal{S}}_m, m \in \mathcal{M}$; hence it only estimates $\{\tilde{\mathbf{h}}_{q,m}\}_{q \in \mathcal{S}_m, m \in \mathcal{M}}$, whereas $\{\hat{\mathbf{h}}_{q,m}\}_{q \in \bar{\mathcal{S}}_m, m \in \mathcal{M}}$ are set to zero; i.e., $\hat{\mathbf{h}}_{q,m} = \mathbf{0}_{\tilde{N}_t}, \forall m \in \mathcal{M}, q \in \bar{\mathcal{S}}_m$. Upon receiving the CSI from all S-RRHs, $\{\hat{\mathbf{h}}_q\}_{q \in \mathcal{Q}}$, the JPCMU computes $\{\tilde{\mathbf{p}}_q\}_{q \in \mathcal{Q}}$, where

$$\tilde{\mathbf{p}}_q \triangleq [\tilde{\mathbf{p}}_{q,1}^\dagger, \dots, \tilde{\mathbf{p}}_{q,M}^\dagger]^\dagger \in \mathbb{C}^{M\tilde{N}_t \times 1} \quad (25)$$

¹¹Under this policy, MSs may remain unserved; i.e., $q \in \bar{\mathcal{S}}_m, \forall m \in \mathcal{M}$. In this case, these MSs can be reallocated at the expense of MSs that are served by the largest number of S-RRHs.

¹²Because the JPCMU knows $\{\alpha_{q,m}\}_{m \in \mathcal{M}, q \in \mathcal{Q}}$ (cf. Assumption 3), it can determine $\bar{\mathcal{S}}_m$ by applying the policy given in Definition 1, and therefore also knows \tilde{N}_t .

is the overall beamformer designated for MS- q .¹³

Definition 2: The P&Q beamformer for MS- q is $\tilde{\mathbf{p}}_q \triangleq \tilde{\mathbf{N}}_q \frac{(\hat{\mathbf{h}}_q^\dagger \tilde{\mathbf{N}}_q)^\dagger}{\|\hat{\mathbf{h}}_q^\dagger \tilde{\mathbf{N}}_q\|}, \forall q \in \mathcal{Q}$, where $\tilde{\mathbf{N}}_q \in \mathbb{C}^{M\tilde{N}_t \times M\tilde{N}_t - (\tilde{Q}_q - 1)}$ is the projection matrix into the null space of $\{\hat{\mathbf{h}}_j \odot (\mathbf{v}_q \otimes \mathbf{1}_{\tilde{N}_t})\}_{j \in \mathcal{Q}-q}$. The factor \tilde{Q}_q is the number of MSs such that $\tilde{\mathbf{h}}_q^\dagger \tilde{\mathbf{h}}_j \neq 0, \forall q, j \in \mathcal{Q}$; i.e., $\tilde{Q}_q = Q - \sum_{j \in \mathcal{Q}-q} \chi_{\{0\}}(M_{q,j})$, where $M_{q,j}$ is the number of S-RRHs that serve both MS- q and MS- j .¹⁴

After setting $\tilde{\mathbf{p}}_q$ according to Definition 2, the JPMCU quantizes $\tilde{\mathbf{p}}_{q,m}$, (cf. (25)) and sends each S-RRH its relevant precoders. Moreover, because $\{\tilde{\mathbf{p}}_{q,m}\}_{q \in \bar{\mathcal{S}}_m, m \in \mathcal{M}} = \mathbf{0}_{\tilde{N}_t}$, the JPMCU does not have to send S-RRH- m the entire set $\{\tilde{\mathbf{p}}_{q,m}\}_{q \in \mathcal{Q}}$, but rather sends $\{\tilde{\mathbf{p}}_{q,m}\}_{q \in \mathcal{S}_m}$, which consists solely of $Q - \bar{Q}$ beamformers. In more explicit terms, it sends the quantization of $\{\tilde{\mathbf{p}}_{q,m}\}_{q \in \mathcal{S}_m}$ to S-RRH- m . Since the latter have a lower dimension $\tilde{N}_t < N_t$, they can be quantized more accurately. Once having received these quantizations, S-RRH- m sets its overall beamformer toward MS- q as

$$\hat{\mathbf{p}}_{q,m}^{\text{P\&Q}} \triangleq \mathbf{A}_m \hat{\mathbf{p}}_{q,m} \in \mathbb{C}^{N_t \times 1} \quad (26)$$

where $\hat{\mathbf{p}}_{q,m}$ denotes the estimate of $\tilde{\mathbf{p}}_{q,m}$.

Definition 3: The overall P&Q beamformer $\hat{\mathbf{p}}_q^{\text{P\&Q}} \in \mathbb{C}^{M\tilde{N}_t} \times 1$ for MS- q is $\hat{\mathbf{p}}_q^{\text{P\&Q}} \triangleq \mathbf{A} \hat{\mathbf{p}}_q$, where $\mathbf{A} = \text{blockdiag}\{\mathbf{A}_1, \mathbf{A}_2, \dots, \mathbf{A}_M\} \in \mathbb{C}^{M\tilde{N}_t \times M\tilde{N}_t}$ and $\hat{\mathbf{p}}_q \triangleq [\hat{\mathbf{p}}_{q,1}^\dagger, \dots, \hat{\mathbf{p}}_{q,M}^\dagger]^\dagger \in \mathbb{C}^{M\tilde{N}_t \times 1}$.

Note that because $\tilde{\mathbf{p}}_q = \tilde{\mathbf{p}}_q \odot (\mathbf{v}_q \otimes \mathbf{1}_{\tilde{N}_t})$ it follows that $\hat{\mathbf{p}}_q = \hat{\mathbf{p}}_q \odot (\mathbf{v}_q \otimes \mathbf{1}_{\tilde{N}_t})$.

Definition 4: Let \mathcal{M}_q be the set of S-RRHs that serve MS- q ; that is, $\mathcal{M}_q = \{m \in \mathcal{M} : q \in \mathcal{S}_m\}$ and denote $M_q = |\mathcal{M}_q|$. Furthermore, let $\mathcal{M}_{q,j} \triangleq \mathcal{M}_q \cap \mathcal{M}_j$ be the set of S-RRHs that serve both MS- q and MS- j , and denote $M_{q,j} = |\mathcal{M}_{q,j}|$.

¹³Since each S-RRH only serves a subset of the MSs, full data sharing is unnecessary. Note that $\tilde{\mathbf{h}}_q$ satisfies $\tilde{\mathbf{h}}_q = \tilde{\mathbf{h}}_q \odot (\mathbf{v}_q \otimes \mathbf{1}_{\tilde{N}_t})$, where \mathbf{v}_q is an M -dimensional vector satisfying $[\mathbf{v}_q]_m = 1$ if S-RRH- m serves MS- q , and 0 otherwise (in the standard scheme every S-RRH serves every MS, hence $\mathbf{v}_q = \mathbf{1}_M, \forall q \in \mathcal{Q}$). Therefore, if $\tilde{\mathbf{p}}_q \neq \tilde{\mathbf{p}}_q \odot (\mathbf{v}_q \otimes \mathbf{1}_{\tilde{N}_t})$, it follows that some S-RRHs, which do not serve MS- q , do transmit s_q . Explicitly, if $\tilde{\mathbf{h}}_{q,m} = \mathbf{0}_{\tilde{N}_t}$ and $\tilde{\mathbf{p}}_{q,m} \neq \mathbf{0}_{\tilde{N}_t}$ for some $m \in \mathcal{M}$, S-RRH- m must transmit the signal s_q , which MS- q does not receive. To avoid transmitting more data than necessary, we set the beamformer $\tilde{\mathbf{p}}_q$ orthogonal to $\{\hat{\mathbf{h}}_j \odot (\mathbf{v}_q \otimes \mathbf{1}_{\tilde{N}_t})\}_{j \in \mathcal{Q}-q}$ from which it follows that $\tilde{\mathbf{p}}_q = \tilde{\mathbf{p}}_q \odot (\mathbf{v}_q \otimes \mathbf{1}_{\tilde{N}_t})$; i.e., the beamformer's weights corresponding to S-RRHs that do not serve MS- q are zero. By not sending $\{s_q\}_{q \in \bar{\mathcal{S}}_m}$ to S-RRH- m , we reduce the number of data streams for that S-RRH to $Q - \bar{Q}$, rather than Q as in the standard scheme.

¹⁴The coefficient \tilde{Q}_q (cf. Definition 2) is the number of MSs served by at least one of the S-RRHs that serve MS- q . $\tilde{Q}_q - 1$ is the number of MSs to which the ZF precoder must zero the interference inflicted by MS- q .

Substituting $\hat{\mathbf{p}}_i^{\text{P\&Q}}$ for $\mathbf{p}_i, i \in \mathcal{Q}$ in (3), MS- q observes the signal

$$y_q = \tilde{\mathbf{h}}_q^\dagger \hat{\mathbf{p}}_q s_q + \sum_{j \in \mathcal{Q}_{-q}} \tilde{\mathbf{h}}_q^\dagger \hat{\mathbf{p}}_j s_j + n_q, \quad \forall q \in \mathcal{Q} \quad (27)$$

where $\tilde{\mathbf{h}}_q = [\tilde{\mathbf{h}}_{q,1}^\dagger, \dots, \tilde{\mathbf{h}}_{q,M}^\dagger]^\dagger$ and $\hat{\mathbf{p}}_q$ is given in Definition 3. We note that $\tilde{\mathbf{h}}_q$ replaces \mathbf{h}_q because each S-RRH applies \mathbf{A}_m (cf. (23)); moreover, the sum runs over \mathcal{Q}_{-q} because of the particular choice of \mathbf{A}_m and $\tilde{\mathbf{p}}_j, j \in \mathcal{Q}$ (Definition 2), as discussed in Footnote 13. The latter can be written as $y_q = \sum_{m \in \mathcal{M}_q} \tilde{\mathbf{h}}_{q,m}^\dagger \hat{\mathbf{p}}_{q,m} s_q + \sum_{j \in \mathcal{Q}_{-q}} \sum_{m \in \mathcal{M}_{q,j}} \tilde{\mathbf{h}}_{q,m}^\dagger \hat{\mathbf{p}}_{j,m} s_j + n_q$, where \mathcal{M}_q and $\mathcal{M}_{q,j}$ are given in Definition 4.

The advantage of the proposed scheme is twofold. From [9], it is known that when quantizing an N -dimensional uncorrelated Rayleigh fading channel with b bits, the quantization error is bounded above by $2^{-\frac{b}{N-1}}$. Therefore, the P&Q has a smaller CSI-quantization error because the channels and beamformers are \tilde{N}_t -dimensional, rather than N_t . Furthermore, since each S-RRH serves fewer MSs, fewer channels and beamformers are delivered to the JPCU and S-RRHs, respectively, through the limited-rate links. Considering an overall budget of B bits for each S-RRH, it follows that the P&Q scheme allocates each channel $B/(Q - \bar{Q})$ bits rather than B/Q in the standard scheme. Consequently, the quantization error is bounded by $2^{-\frac{B}{(Q-\bar{Q})(\tilde{N}_t-1)}}$ rather than by $2^{-\frac{B}{Q(\tilde{N}_t-1)}}$. The second advantage of the P&Q scheme is in reducing fronthaul data load, which is a major problem in C-RAN. This reduction is because each S-RRH serves only $Q - \bar{Q}$ MSs. Hence, fewer data signals must be transferred via the fronthaul between the BBU to each S-RRH. Moreover, because each S-RRH now serves fewer MSs, the overall power allocated for each MS may be increased.

V. THE P&Q SCHEME: PERFORMANCE ANALYSIS

We now present results corresponding to Theorem 1 and Corollary 4 for the P&Q scheme. We assume the following.

Assumption 7: Each S-RRH serves $Q - \bar{Q}$ MSs with $\tilde{P}_{q,m} = \tilde{P} = \frac{P_{\max}}{Q - \bar{Q}}, \forall q \in \mathcal{Q}, m \in \mathcal{M}$.

Because the analysis of the P&Q is more complicated than the standard scheme, we simplify the setup as follows.

Assumption 8 (symmetric system-geometry with an equal pathloss constrain): The long-term channel attenuation satisfies $\alpha_{q,m} = 1/M, \forall q \in \mathcal{Q}, m \in \mathcal{M}$.

This assumption holds, e.g., if one places S-RRHs on the edges of a regular polygon with M nodes and MSs close to each other at the center of that polygon.¹⁵ Then, MSs have approximately the same long-term channel attenuation to each S-RRH. In a rich scattering environment, the MSs will experience independent fading.¹⁶

Definition 5: Consider Assumptions 7 and 8, let $\Delta\tilde{R}_q \triangleq R_q^* - \hat{R}_q$ be the P&Q rate-gap where R_q^* is given in (11), $\hat{R}_q = \mathbb{E}\{\log(1 + \text{SINR}_q(\{\hat{\mathbf{p}}_i^{\text{P\&Q}}\}_{i \in \mathcal{Q}}))\}$, and $\text{SINR}_q(\cdot)$ is defined similarly to (9) with $\hat{\mathbf{p}}_i^{\text{P\&Q}}$ as its argument (cf. Definition 3) while substituting \tilde{P} for P .

Definition 6: Let $\tilde{\mathbf{p}}_q^*$ be the P&Q beamformer without quantization error; i.e., $\tilde{\mathbf{p}}_q^*$ is obtained by replacing $\hat{\mathbf{h}}_q$ with $\tilde{\mathbf{h}}_q$ in $\tilde{\mathbf{p}}_q$ (cf. Definition 2) as well as in the calculation of $\tilde{\mathbf{N}}_q$. We further denote the P&Q inherent rate-loss by $\Delta R_{\text{AG},q} \triangleq R_q^* - \tilde{R}_q^*$ where R_q^* is given in (11) and $\tilde{R}_q^* = \mathbb{E}\{\log(1 + \tilde{P}|\tilde{\mathbf{h}}_q^\dagger \tilde{\mathbf{p}}_q^*|^2)\}$. In other words, $\Delta R_{\text{AG},q}$ is the difference between the standard-scheme and P&Q-scheme rates without quantization errors, resulting from the loss in array gain.

Theorem 5: Consider Assumptions 1, 3 to 5, 7 and 8, and assume that the P&Q (cf. Definition 2) is applied with B bits, (cf. Assumptions 4 and 5), where $\tilde{\mathbf{h}}_{q',m}$, $\tilde{\mathbf{p}}_{q',m}$ are quantized using RVQ with $B/(Q - \bar{Q})$ (assumed integer) bits $\forall q' \in \mathcal{Q}, \forall m \in \mathcal{M}$. Then, the MS- q , $q \in \mathcal{Q}$ expected throughput-loss due to CSI quantization, in comparison to a perfect CSI, satisfies

$$\Delta\tilde{R}_q \leq \Delta\tilde{R}_{1,q} + \Delta\tilde{R}_{2,q} + \Delta R_{\text{AG},q} \quad (28)$$

where

$$\begin{aligned} \Delta\tilde{R}_{1,q} \triangleq & \log \left\{ 1 + \tilde{P} \left[\sum_{j \in \mathcal{Q}-q} \frac{\tilde{N}_t M_{q,j}}{M_j M} \right] \times \left[\frac{1}{\tilde{N}_t - 1} 2^{\frac{-B}{(Q-\bar{Q})(\tilde{N}_t-1)}} \left(2(1 - \mathcal{U}(2^{\frac{B}{Q-\bar{Q}}}, \tilde{a})) + 2^{\frac{-B}{(Q-\bar{Q})(\tilde{N}_t-1)}} \right) \right. \right. \\ & \left. \left. + (1 - \mathcal{U}(2^{\frac{B}{Q-\bar{Q}}}, \tilde{a}))^2 - (1 - \mathcal{U}(2^{\frac{B}{Q-\bar{Q}}}, \tilde{a})/2 - \mathcal{U}(2^{\frac{B}{Q-\bar{Q}}}, 2\tilde{a}))^4 \right] \right\} \end{aligned} \quad (29)$$

$$\begin{aligned} \Delta\tilde{R}_{2,q} \triangleq & 6\tilde{R}_q^* (\mathcal{U}(2^{\frac{B}{Q-\bar{Q}}}, \tilde{a}) + \mathcal{V}_{M_q}(2^{\frac{B}{Q-\bar{Q}}}, \tilde{a})) \\ & + \frac{\pi \tilde{P} \tilde{N}_t}{\sqrt{\tilde{P} \tilde{N}_t + 1}} (\mathcal{U}(2^{\frac{B}{Q-\bar{Q}}}, \tilde{a}/2) + \mathcal{V}_{M_q}(2^{\frac{B}{Q-\bar{Q}}}, \tilde{a}/2)) \end{aligned} \quad (30)$$

¹⁵In more explicit terms, S-RRHs are placed at $\mathcal{G} = \{(r \cos(2\pi m/M), r \sin(2\pi m/M)) \in \mathbb{R}^2 : m \in \{0, \dots, M-1\}\}$, where $r > 0$ is fixed where $(0, 0)$ is the center of the polygon. The MSs are placed very close to each other around the point $(0, 0)$.

¹⁶This happens as long as the distance between them is larger than the wavelength; which is a very reasonable since cellular wavelengths are typically on the order of centimeters.

Here, $\tilde{a} = \frac{1}{\tilde{N}_t - 1}$, $\tilde{P} = \frac{P_{\max}}{Q - \tilde{Q}}$, $M_q, M_{q,j}$ are in Definition 4 and $\mathcal{U}(\cdot)$, $\mathcal{V}_M(\cdot)$ are defined in Theorem 1. Furthermore, the term $\Delta R_{AG,q}$ (cf. (28) as well as Definition 6) satisfies

$$\Delta R_{AG,q} = \varphi(T, P/M) - \varphi(\tilde{T}_q, \tilde{P}/M) \quad (31)$$

where $\varphi(\cdot)$ and T are in (18), $\tilde{T}_q = M_q \tilde{N}_t - (\tilde{Q}_q - 1)$, and \tilde{Q}_q is in Definition 2.

Proof: Similar to (19), it can be shown that

$$\Delta \tilde{R}_q \leq \tilde{A}_1 + \Delta R_{AG,q} - \tilde{A}_2 + \tilde{A}_3 \quad (32)$$

where $\tilde{A}_1 = \mathbb{E}\{\log(1 + \tilde{P} |\tilde{\mathbf{h}}_q^\dagger \tilde{\mathbf{p}}_q^*|^2)\}$, $\tilde{A}_2 = \mathbb{E}\{\log(1 + \tilde{P} |\tilde{\mathbf{h}}_q^\dagger \hat{\mathbf{p}}_q|^2)\}$, $\tilde{A}_3 = \mathbb{E}\{\log(1 + \tilde{P} \sum_{j \in \mathcal{Q}_q} |\tilde{\mathbf{h}}_q^\dagger \hat{\mathbf{p}}_j|^2)\}$ and the additional term is given by $\Delta R_{AG,q} = A_1 - \tilde{A}_1$ where A_1 is defined in (19). The proof then follows from the following lemmas.

Lemma 6: Under the assumptions of Theorem 5, $\tilde{A}_3 \leq \Delta \tilde{R}_{1,q}$, and $\tilde{A}_1 - \tilde{A}_2 \leq \Delta \tilde{R}_{2,q}$ (cf. (29), (30), (32)).

Proof: See Appendix C. ■

After substituting the inequalities of Lemma 6 into (32) it remains to show (31). To this end, we use $R^* = \varphi(T, P/M)$ (cf. (18)) and $\tilde{A}_1 = \varphi(\tilde{T}_q, \tilde{P}/M)$, obtained by applying the former while replacing T and P with \tilde{T}_q and \tilde{P} , respectively. ■

Definition 7 (Symmetric selection policy): For $Q/M \in \mathbb{N}$ and $M\bar{Q}/Q \in \mathbb{N}$, let $\{\mathcal{Q}_m\}_{m=1}^M$ be a partition of \mathcal{Q} , such that $|\mathcal{Q}_m| = Q/M \forall m$. In this selection policy, $\forall m \in \mathcal{M}$, the set of MSs discarded by S-RRH- m , is $\bar{\mathcal{S}}_m = \bigcup_{i=1}^{\bar{Q}M/Q} \mathcal{Q}_{(i+m) \bmod M}$.

Corollary 7: Consider the assumptions of Theorem 5 and assume in addition that $Q/M \in \mathbb{N}$, $M\bar{Q}/Q \in \mathbb{N}$ and a symmetric selection-policy (cf. Definition 7). Then $\Delta \tilde{R} \leq \Delta \tilde{R}_1 + \Delta \tilde{R}_2 + \Delta R_{AG}$, where $\Delta R_{AG} = \varphi(T, P/M) - \varphi(\tilde{T}, \tilde{P}/M)$, $\tilde{T} = M(1 - \bar{Q}/Q)\tilde{N}_t + 1 - \min(Q, (2 - 1/M)Q - 2\bar{Q})$, and

$$\Delta \tilde{R}_1 = \log \left\{ 1 + \frac{\tilde{P}\tilde{N}_t(Q - \bar{Q} - 1)}{M} \times \left[\frac{1}{\tilde{N}_t - 1} 2^{\frac{-B}{(Q-\bar{Q})(\tilde{N}_t-1)}} \left(2(1 - \mathcal{U}(2^{\frac{B}{Q-\bar{Q}}}, \tilde{a})) + 2^{\frac{-B}{(Q-\bar{Q})(\tilde{N}_t-1)}} \right) \right. \right. \\ \left. \left. + (1 - \mathcal{U}(2^{\frac{B}{Q-\bar{Q}}}, \tilde{a}))^2 - (1 - \mathcal{U}(2^{\frac{B}{Q-\bar{Q}}}, \tilde{a})/2 - \mathcal{U}(2^{\frac{B}{Q-\bar{Q}}}, 2\tilde{a}))^4 \right] \right\} \quad (33)$$

$$\Delta \tilde{R}_2 = 6\varphi(\tilde{T}, \tilde{P}/M) [\mathcal{U}(2^{\frac{B}{Q-\bar{Q}}}, \tilde{a}) + \mathcal{V}_{(1-\bar{Q}/Q)M}(2^{\frac{B}{Q-\bar{Q}}}, \tilde{a})] \\ + \frac{\pi\tilde{P}\tilde{N}_t}{\sqrt{\tilde{P}\tilde{N}_t + 1}} [\mathcal{U}(2^{\frac{B}{Q-\bar{Q}}}, \tilde{a}/2) + \mathcal{V}_{(1-\bar{Q}/Q)M}(2^{\frac{B}{Q-\bar{Q}}}, \tilde{a}/2)] \quad (34)$$

Proof: Due to space limitations, we provide here an outline of the proof (a detailed proof is given in [34] Supplementary B). The first step shows that the sum in (29) runs over constant terms, and can therefore be replaced by a factor $Q - \bar{Q} - 1$ in (33). To this end, one must show that $M_q = (1 - \bar{Q}/Q)M, \forall q \in \mathcal{Q}$. Finally, we substitute the latter result for \tilde{T}_q in (31) and obtain $\tilde{T}_q = \tilde{T}$, where \tilde{T} is given in this corollary. ■

Remark 2: Under the suppositions of Corollary 7, all MS rates are equal, $\hat{R}_q = \hat{R}$ (cf. Definition 5), and satisfy $\hat{R} \geq R^* - \Delta\bar{R}_1 - \Delta\bar{R}_2 - \Delta R_{AG}$, where R^* is given in (18). Moreover, considering the standard scheme under Assumption 8 and $Q/M \in \mathbb{N}$, it follows that $\hat{R} \geq R^* - \Delta\bar{R}_1 - \Delta\bar{R}_2$.

Next, similar to Corollary 4, we have have following corollary.

Corollary 8: Consider $\Delta\bar{R}_1$ and $\Delta\bar{R}_2$, given in Corollary 7. Then the bound $\tilde{\Delta}R \leq \Delta\bar{R}_1 + \Delta\bar{R}_2 + \Delta R_{AG}$ in (28) can be further approximated as

$$\Delta\bar{R}_1 + \Delta\bar{R}_2 = 2^{\frac{-B}{2(Q-\bar{Q})(\tilde{N}_t-1)}} \frac{\pi \tilde{P} \tilde{N}_t}{\sqrt{\tilde{P} \tilde{N}_t + 1}} \left[V_M \left(\frac{1/2}{\tilde{N}_t - 1} \right) + \Gamma \left(\frac{1/2}{\tilde{N}_t - 1} + 1 \right) \right] + O(2^{\frac{-2B}{(Q-\bar{Q})(\tilde{N}_t-1)}}) \quad (35)$$

Proof: The proof is identical to the proof of Corollary 4. ■

We conclude this section with a discussion and insights. By examining Corollaries 4 and 8, it follows that the rate loss ΔR in the standard scheme (which here is not a function of q , cf. Remark 2) approaches zero as B increases. . In contrast, the rate gap in the P&Q scheme, $\Delta\tilde{R}$, is bounded away from zero. Explicitly, it approaches $\Delta R_{AG} > 0$ (cf. Definition 6), which is independent of B and is due to the array-gain loss induced by the dimension reduction. However, the other terms $\Delta\bar{R}_1 + \Delta\bar{R}_2$, comprising $\Delta\tilde{R}$, decrease to zero much faster than $\Delta\bar{R}_1 + \Delta\bar{R}_2$ (cf. (20) and (35)); therefore, $\Delta\tilde{R}$ approaches ΔR_{AG} much faster than ΔR approaches zero. Subsequently, \hat{R} approaches $R^* - \Delta R_{AG}$, much faster than \hat{R} approaches R^* . The final observation is that \hat{R} can be higher than \hat{R} as long as ΔR is more significant than ΔR_{AG} . Numerical results presented in the subsequent section indicate that \hat{R} is indeed higher than \hat{R} for a wide range of quantization bits.

VI. NUMERICAL RESULTS

In this section, we study two setups. The first consider setups matching the theoretical analysis in Sections III and V, where we compare the derived bounds to their corresponding Monte Carlo

(MC) simulations (Fig. 2). The second is a practically oriented setup in which the MSs are placed randomly in the plane with a more realistic channel model (cf. Fig. 3).

Beginning with the theoretical analysis setups, Figures 2(a) and 2(b) depict the standard-scheme performance (ergodic rate), evaluated via MC (10^4 channel realizations), compared to the rate bound described in Remark 2.¹⁷ Also included is the rate under perfect CSI (cf. (18)). Considering that transmitters could always turn off some of their antennas if it yields a higher rate, for each B , we picked $N_t \in \{2, \dots, 8\}$ with the maximum rate. The corresponding bound was also maximized over N_t for each B .

In Fig. 2(a) we considered $Q = 2$ MSs placed at $(-80,0)$ and $(80,0)$ (in meters), served by $M = 4$ S-RRHs. We placed an S-RRH for each $m \in \{1, \dots, M\}$ such that its x-y coordinates are the real and imaginary of $80e^{j\pi(1+2m)/4}$, respectively (in meters). Note that $\alpha_q = \sum_m \alpha_{q,m}$ is equal for $q \in \{1, 2\}$. We used a path-loss exponent of 3.5 and set the power according to Assumption 6 such that $\alpha_q P_{\max}$ (cf. Theorem 1) is 35 dB (black) and 15 dB (blue). Fig. 2(b) considers a symmetric network that satisfies Assumption 8 with $M = 4$ S-RRHs and $Q = 8$ MSs with a similar power allocation. The results show that the bound gets tighter as B increases. Moreover, the bound exhibits the same behavior as the MC simulation when B increases. We note that the curves are not smooth since we allowed antenna turn off. The curve is unsmooth for bit numbers in which N_t yielding the highest rate varies.

Fig. 2(c) compares the P&Q and the standard schemes for the same setup as Fig. 2(b) with $P_{\max} = 35$ dB; hence the black curves are the same in both figures, except of the horizontal logarithmic scale. We calculated the P&Q rate bound using Corollary 7, and evaluated the P&Q scheme rate via MC (10^4 channel realizations) where we maximized it also over all feasible values of \bar{Q} . The result indicates that the P&Q scheme provides a significant performance gain; that is, $\hat{\hat{R}}$ is much greater than \hat{R} for at least 250 bits. Moreover, in the P&Q scheme, the bound is tighter and approaches the MC simulation way faster than the corresponding bound in the standard scheme.

To further investigate the P&Q scheme, we study a practically oriented setup with randomly dispersed MSs while considering propagation loss and shadowing. The format includes a cluster

¹⁷In cases where there is a closed-form expression for the rate under perfect CSI, the rate lower-bound follows by subtracting the rate gap from the perfect-CSI rate.

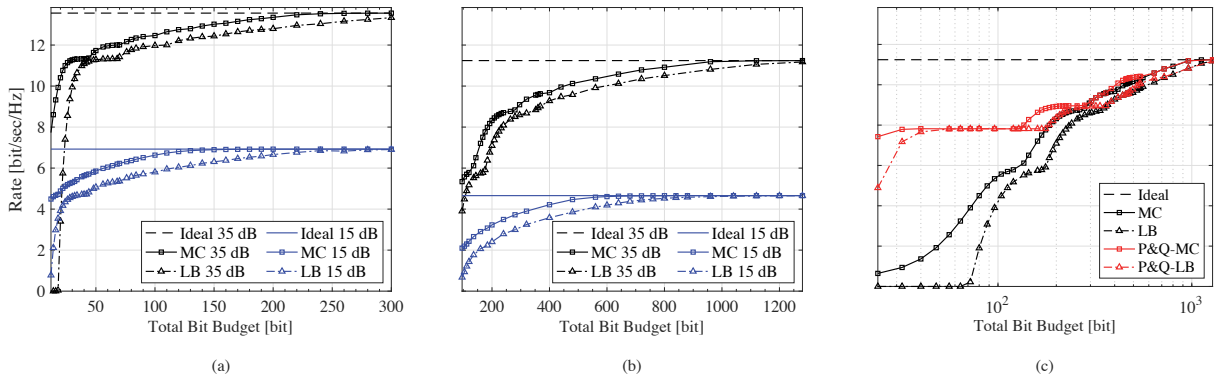


Fig. 2. Averaged throughput lower bounds (cf. Remark 2) and MC simulation, as a function of the overall bit budget B for $N_t = 8$ antennas and $M = 4$ S-RRHs, and equal transmit-power to each MS. Fig (a) considers $Q = 2$ MSs with non-equal pathlosses to each S-RRH, (b) presents the symmetric configuration (cf. Assumption 8) of $Q = 8$ MSs. In (c), we compare the P&Q (red) to the standard scheme (black) for the same setup as in (b) with $P = 35$ dB; hence the black curve is the same as in (b) but in a logarithmic scale. The vertical axis is the same in all figures.

of $M = 4$ S-RRHs creating a 100 m edge-length rhombus with an edge angle of 120° . Each S-RRH is equipped with $N_t = 8$ isotropic transmit antennas. Eight single-antenna MSs ($Q = 8$) were placed uniformly at random in the common area spanned by four hexagons, each one centered at a different S-RRH. We set a minimum distance of 10 m between each MS and S-RRH. The results were averaged over 20 realizations of MS-placements, where each realization determined a set of attenuation factors $\alpha = \{\alpha_{q,m} : q = 1 \cdots 8, m = 1 \cdots 4\}$ according $\alpha_{q,m} = -128 - 37.6 \log_{10}(r_{q,m})$ (in dB),¹⁸ where $r_{q,m}$ is the distance from S-RRH- m to MS- q in Km. The noise level at the receivers was -121 dBm. For each realization of MS-placement, we calculated each MS rate by averaging over 40 channel realizations. In calculating the network throughput, we averaged the rates of all MSs across all placements. To ensure a fair comparison, we considered that the transmitters could always turn off some antennas to reduce the effective MISO channel dimensions. Accordingly, in the standard scheme, we maximized the rate over N_t , whereas, in the P&Q scheme, we maximized the rate over \bar{Q} while keeping $N_t = 8$. Finally, we set the overall power, transmitted to each MS, fixed; i.e., $P_q = P_{q'}, \forall q, q' \in \mathcal{Q}$ (cf. (3)). To maintain $\|\mathbf{p}_q\| = 1$, each S-RRH had to backoff its power until none was violating its individual

¹⁸This model was used for urban-area non-line-of-site links by the 3GPP; cf. page 61 3GPP Technical Report 36.814 [35].

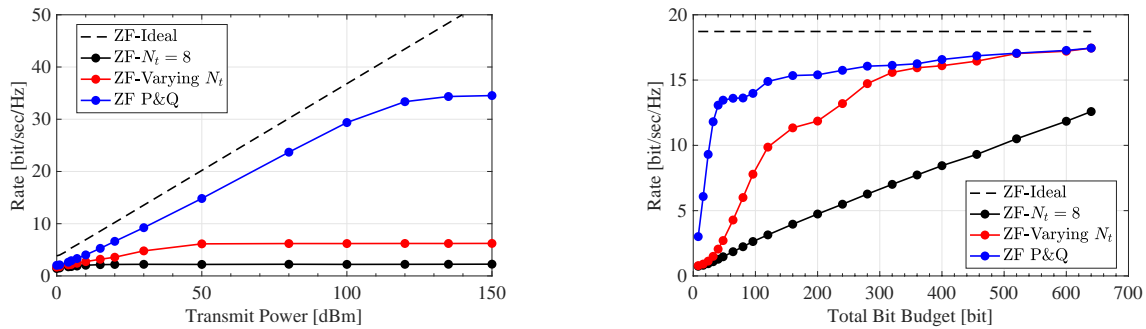
(a) Throughput vs. P_{\max} for $B = 176$ bits.(b) Throughput vs. B for $P_{\max} = 37$ dBm.

Fig. 3. Throughput of the P&Q scheme (blue), standard scheme with varying N_t (red), with fixed $N_t = 8$ (black), and under perfect CSI (dashed). We equally allocated the overall bit budget per S-RRH, B (cf. Assumptions 4 and 5) to each MS; that is, B/Q and $B/(Q - \bar{Q})$ bits per MS in the standard and in the P&Q scheme, respectively, where non-integer values were floored.

power constraint P_{\max} .¹⁹ A more detailed description of this policy is given in ([34]).

Fig. 3(a) presents the throughput as a function of each S-RRH transmit power, P_{\max} (cf. Assumption 2). The results show that the P&Q significantly outperformed the standard scheme. In the latter, the network is already interference-limited at 50 dBm, whereas in the former, at 110 dBm. Therefore, while the perfect-CSI throughput in the standard scheme is higher than the P&Q counterpart, the latter goes up much faster.

Fig. 3(b) presents the average throughput as a function of B under a per-S-RRH power constraint of $P_{\max} = 45$ dBm to study the effect of the quantization bits. The result shows that the P&Q throughput rapidly increases with B ; thus, outperforming the standard scheme for a wide range of B .

VII. CONCLUSIONS

This article makes two contributions. The first is a new upper bound on the rate degradation experienced by a cluster of S-RRHs, that employ joint ZF with incomplete CSI compared to perfect CSI. The second is a new CSI sharing scheme that aims to reduce the CSI overhead on the links between S-RRHs in C-RAN. The key distinguishing characteristic of this scheme is

¹⁹Note that while this power allocation strategy is not optimal, it yields good performance in high SNRs.

that it applies front-end matrices prior to CSI quantization to create designated effective channels of low dimensionality; hence can be quantized more accurately with fewer bits. Furthermore, each S-RRH serves fewer MSs, thus reducing CSI and the number of data streams delivered. We demonstrated, through analytical analysis and simulation, that the proposed scheme achieves a significant performance gain.

Possible extensions of this work would be to optimize the power allocation for each MS and optimize the dimension reduction level; i.e., \bar{Q} (cf. Definition 1). Finally, it is necessary to explore channel models beyond independent Rayleigh fading.

APPENDIX A

To prove Lemma 2, we begin by rewriting the decomposition in (7) as

$$\bar{\mathbf{h}}_{q,m} = \hat{\mathbf{h}}_{q,m} \cos \theta_{q,m} + \mathbf{s}_{q,m} \sin \theta_{q,m}, \quad (36)$$

where $\bar{\mathbf{h}}_{q,m} = \mathbf{h}_{q,m} / \|\mathbf{h}_{q,m}\|$ and $\hat{\mathbf{h}}_{q,m} = \hat{\mathbf{h}}_{q,m} / \|\hat{\mathbf{h}}_{q,m}\|$, $\theta_{q,m}$ is the angle between $\bar{\mathbf{h}}_{q,m}$ and $\hat{\mathbf{h}}_{q,m}$, and $\mathbf{s}_{q,m} \in \mathbb{C}^{N_t \times 1}$ is a unit-norm random vector that is uniformly distributed over the null space of $\hat{\mathbf{h}}_{q,m}$ [9]. Moreover, we define²⁰

$$\hat{\mathbf{p}}_{j,m} = \bar{\mathbf{p}}_{j,m} \cos \phi_{j,m} + \mathbf{g}_{j,m} \sin \phi_{j,m} \quad (37)$$

where $\bar{\mathbf{p}}_{j,m} = \mathbf{p}_{j,m} / \|\mathbf{p}_{j,m}\|$ and $\hat{\mathbf{p}}_{j,m} = \hat{\mathbf{p}}_{j,m} / \|\hat{\mathbf{p}}_{j,m}\|$, $\phi_{j,m}$ is the angle between $\bar{\mathbf{p}}_{j,m}$ and $\hat{\mathbf{p}}_{j,m}$, and $\mathbf{g}_{j,m} \in \mathbb{C}^{N_t \times 1}$ is a unit-norm random vector that is uniformly distributed over the null space of $\bar{\mathbf{p}}_{j,m}$. Applying Jensen's inequality to A_3 , one obtains

$$A_3 \leq \log \left(1 + P \sum_{j \in \mathcal{Q}_q} \mathbb{E} \{ |\mathbf{h}_q^\dagger \hat{\mathbf{p}}_j|^2 \} \right) \quad (38)$$

and using (36) and (37), the term with the expectation in (38) can be written as

$$\begin{aligned} \mathbb{E} \{ |\mathbf{h}_q^\dagger \hat{\mathbf{p}}_j|^2 \} &= \mathbb{E} \left\{ \left| \sum_{m=1}^M \bar{\mathbf{h}}_{q,m}^\dagger \hat{\mathbf{p}}_{j,m} \|\mathbf{h}_{q,m}\| \|\hat{\mathbf{p}}_{j,m}\| \right|^2 \right\} = \mathbb{E} \left\{ \left| \sum_{m=1}^M \left(\hat{\mathbf{h}}_{q,m}^\dagger \mathbf{p}_{j,m} \Lambda_{1,1m} \right. \right. \right. \\ &\quad \left. \left. \left. + \hat{\mathbf{h}}_{q,m}^\dagger \mathbf{g}_{j,m} \|\hat{\mathbf{p}}_{j,m}\| \Lambda_{1,2m} + \mathbf{s}_{q,m}^\dagger \mathbf{p}_{j,m} \|\mathbf{h}_{q,m}\| \Lambda_{2,1m} + \mathbf{s}_{q,m}^\dagger \mathbf{g}_{j,m} \|\mathbf{h}_{q,m}\| \|\hat{\mathbf{p}}_{j,m}\| \Lambda_{2,2m} \right) \right|^2 \right\} \end{aligned} \quad (39)$$

where $\Lambda_{k,lm} = C_k(\theta_{q,m})C_l(\phi_{j,m})$, $k, l \in \{1, 2\}$ and $C_1(\theta) = \cos \theta$, $C_2(\theta) = \sin \theta$. Extending (39), one obtains

$$\mathbb{E} \{ |\mathbf{h}_q^\dagger \hat{\mathbf{p}}_j|^2 \} = D + E + F + G + H \quad (40)$$

²⁰Interchanging $\bar{\mathbf{p}}_{j,m}$ and $\hat{\mathbf{p}}_{j,m}$ yields an equivalent decomposition of the quantized beamforming vector [36]; furthermore, $\hat{\mathbf{p}}_{j,m}$ is uniformly distributed.

where $D = \mathbb{E}\left\{\left|\sum_{m=1}^M \hat{\mathbf{h}}_{q,m}^\dagger \mathbf{p}_{j,m} \Lambda_{1,1,m}\right|^2\right\}$, $E = \mathbb{E}\left\{\left|\sum_{m=1}^M \hat{\mathbf{h}}_{q,m}^\dagger \mathbf{g}_{j,m} \|\hat{\mathbf{p}}_{j,m}\| \Lambda_{1,2,m}\right|^2\right\}$, $F = \mathbb{E}\left\{\left|\sum_{m=1}^M \mathbf{s}_{q,m}^\dagger \mathbf{p}_{j,m} \|\mathbf{h}_{q,m}\| \Lambda_{2,1,m}\right|^2\right\}$, $G = \mathbb{E}\left\{\left|\sum_{m=1}^M \mathbf{s}_{q,m}^\dagger \mathbf{g}_{j,m} \|\mathbf{h}_{q,m}\| \|\hat{\mathbf{p}}_{j,m}\| \Lambda_{2,2,m}\right|^2\right\}$ and $H = \sum_{i=1}^{12} \Xi_i$ in which $\{\Xi_i\}_{i=1}^{12}$ includes all non-quadratic terms resulting from the extension of the right-hand side (r.h.s.) of (39); i.e., terms that cannot be written as $|\cdot|^2$. For example, Ξ_1 is given by

$$\Xi_1 = \mathbb{E}\left\{\sum_{m=1}^M \sum_{n=1}^M \hat{\mathbf{h}}_{q,m}^\dagger \mathbf{p}_{j,m} \mathbf{g}_{j,n}^\dagger \hat{\mathbf{h}}_{q,n} \|\hat{\mathbf{p}}_{j,n}\| \Lambda_{1,1,m} \Lambda_{1,2,n}\right\} \quad (41)$$

Proposition 9: The term D , in (40), satisfies

$$D \leq \frac{\alpha_q N_t}{M} \left((1 - \mathcal{U}(2^{B/Q}, a))^2 - (1 - \mathcal{U}(2^{B/Q}, a)/2 - \mathcal{U}(2^{B/Q}, 2a))^4 \right) \quad (42)$$

where $a = \frac{1}{N_t - 1}$ and $\mathcal{U}(\cdot)$ is defined in (16).

Proof: Because $\{\Lambda_{1,1,m}\}_{m \in \mathcal{M}}$ are identically distributed, it can be written as $\Lambda_{1,1,m} = \sigma + \bar{\Lambda}_{1,1,m}$, $\forall m \in \mathcal{M}$, where $\mathbb{E}\{\bar{\Lambda}_{1,1,m}\} = 0$ and $\sigma = \mathbb{E}\{\Lambda_{1,1,m}\}$. Substituting $\Lambda_{1,1,m}$ into D (cf. (40)) while recalling that $\{\theta_{q,i}, \phi_{j,i}\}_{i \in \mathcal{M}, q, j \in \mathcal{Q}}$, are independent of $\{\hat{\mathbf{h}}_{q,i}, \mathbf{p}_{j,i}\}_{i \in \mathcal{M}, q, j \in \mathcal{Q}}$, it can be shown that

$$D = \sigma^2 \mathbb{E}\left\{\left|\hat{\mathbf{h}}_q^\dagger \mathbf{p}_j\right|^2\right\} + \mathbb{E}\left\{\left|\sum_{m=1}^M \hat{\mathbf{h}}_{q,m}^\dagger \mathbf{p}_{j,m} \bar{\Lambda}_{1,1,m}\right|^2\right\} \quad (43)$$

$$\begin{aligned} & + \sigma \sum_{m=1}^M \sum_{n=1}^M \mathbb{E}\left\{\hat{\mathbf{h}}_{q,m}^\dagger \mathbf{p}_{j,m} \mathbf{p}_{j,n}^\dagger \hat{\mathbf{h}}_{q,n}\right\} \mathbb{E}\{\bar{\Lambda}_{1,1,n}\} + \sigma \sum_{m=1}^M \sum_{n=1}^M \mathbb{E}\left\{\hat{\mathbf{h}}_{q,m}^\dagger \mathbf{p}_{j,m} \mathbf{p}_{j,n}^\dagger \hat{\mathbf{h}}_{q,n}\right\} \mathbb{E}\{\bar{\Lambda}_{1,1,m}\} \\ & = \mathbb{E}\left\{\left|\sum_{m=1}^M \hat{\mathbf{h}}_{q,m}^\dagger \mathbf{p}_{j,m} \bar{\Lambda}_{1,1,m}\right|^2\right\} \end{aligned} \quad (44)$$

To obtain the latter, we also used $\hat{\mathbf{h}}_q^\dagger \mathbf{p}_j = 0$, $\forall j \neq q \in \mathcal{Q}$ and $\mathbb{E}\{\bar{\Lambda}_{1,1,m}\} = 0$. Hence

$$D = \mathbb{E}\left\{\sum_{m=1}^M \left|\hat{\mathbf{h}}_{q,m}^\dagger \mathbf{p}_{j,m}\right|^2 \bar{\Lambda}_{1,1,m}^2\right\} + \mathbb{E}\left\{\sum_{m=1}^M \sum_{n \neq m}^M \hat{\mathbf{h}}_{q,m}^\dagger \mathbf{p}_{j,m} \mathbf{p}_{j,n}^\dagger \hat{\mathbf{h}}_{q,n} \bar{\Lambda}_{1,1,m} \bar{\Lambda}_{1,1,n}\right\} \quad (45)$$

$$= \sum_{m=1}^M \underbrace{\mathbb{E}\left\{\|\mathbf{p}_{j,m}\|^2 \|\hat{\mathbf{h}}_{q,m}\|^2 \left|\hat{\mathbf{h}}_{q,m}^\dagger \bar{\mathbf{p}}_{j,m}\right|^2\right\}}_{I_{q,m}} \underbrace{\mathbb{E}\left\{\bar{\Lambda}_{1,1,m}^2\right\}}_J \quad (46)$$

where we again used the independence between $\{\theta_{q,i}, \phi_{j,i}\}_{i \in \mathcal{M}, q, j \in \mathcal{Q}}$ and $\{\hat{\mathbf{h}}_{q,i}, \mathbf{p}_{j,i}\}_{i \in \mathcal{M}, q, j \in \mathcal{Q}}$ as well as the independence between $\bar{\Lambda}_{1,1,m}$ and $\bar{\Lambda}_{1,1,n}$ $\forall m \neq n \in \mathcal{M}$.

Next, using $I_{q,m} = \sqrt{I_{q,m}^2}$ and applying the Cauchy-Schwarz inequality, one obtains

$$I_{q,m} \leq \sqrt{\mathbb{E}^2\{\|\mathbf{p}_{j,m}\|^2\} \mathbb{E}^2\{\|\hat{\mathbf{h}}_{q,m}\|^2\} \mathbb{E}^2\left\{\left|\hat{\mathbf{h}}_{q,m}^\dagger \bar{\mathbf{p}}_{j,m}\right|^2\right\}} \stackrel{(a)}{=} \frac{\alpha_{q,m} N_t}{M} \mathbb{E}\left\{\left|\hat{\mathbf{h}}_{q,m}^\dagger \bar{\mathbf{p}}_{j,m}\right|^2\right\} \stackrel{(b)}{\leq} \frac{\alpha_{q,m} N_t}{M} \quad (47)$$

wherein (a) we used Assumption 1, $E\{\|\hat{\mathbf{h}}_{q,m}\|^2\}/\alpha_{q,m} = N_t$ [9], and $E\{\|\mathbf{p}_{j,m}\|^2\} = \frac{1}{M}$. The latter follows because $\|\mathbf{p}_j\|^2 = 1$ and $\{\|\mathbf{p}_{j,m}\|\}_{m \in \mathcal{M}}$ are identically distributed. In (b) we used $E\{|\hat{\mathbf{h}}_{q,m}^\dagger \bar{\mathbf{p}}_{j,m}|^2\} \leq 1$. Proceeding to J (cf. (46)), note that

$$\begin{aligned} J &= E\{(\Lambda_{1,1_m} - E\{\Lambda_{1,1_m}\})^2\} = E\{\cos^2 \theta_{q,m} \cos^2 \phi_{j,m}\} - (E\{\cos \theta_{q,m} \cos \phi_{j,m}\})^2 \\ &= E^2\{\cos^2 \theta_{q,m}\} - E^4\{\cos \theta_{q,m}\}, \end{aligned} \quad (48)$$

where the latter follows since $\theta_{q,m}$ and $\phi_{j,m}$, $\forall m \in \mathcal{M}$, $q, j \in \mathcal{Q}$, are independent identically distributed. Because $\mathbf{h}_{q,m}$ is quantized with B/Q bits, it follows that [9]

$$E\{\cos^2 \theta_{q,m}\} = 1 - \mathcal{U}(2^{B/Q}, a) \quad (49)$$

where \mathcal{U} is defined in (16). Before continuing, note that

$$E\{\cos \theta_{q,m}\} \geq 1 - \mathcal{U}(2^{B/Q}, a)/2 - \mathcal{U}(2^{B/Q}, 2a) \quad (50)$$

where we used $\cos \theta_{q,m} = \sqrt{1 - \sin^2(\theta_{q,m})}$ and the inequality $\sqrt{1-x} \geq 1 - x/2 - x^2$, $\forall x \in [0, 1]$. Thus, $J \leq (1 - \mathcal{U}(2^{B/Q}, a))^2 - (1 - \mathcal{U}(2^{B/Q}, a)/2 - \mathcal{U}(2^{B/Q}, 2a))^4$, which together with $\sum_{m=1}^M \alpha_{q,m} = \alpha_q$ (cf. Theorem 1) establishes the desired result. ■

Proposition 10: The terms E and F , given in (40), satisfy

$$E, F \leq \frac{\alpha_q N_t}{M(N_t - 1)} (1 - \mathcal{U}(2^{B/Q}, a)) 2^{\frac{-B}{Q(N_t - 1)}} \quad (51)$$

Proof: Rewriting E (cf. (40)) one obtains

$$E = E\left\{ \sum_{m=1}^M |\hat{\mathbf{h}}_{q,m}^\dagger \mathbf{g}_{j,m} \|\hat{\mathbf{p}}_{j,m}\|^2 \Lambda_{1,2_m}^2 \right\} \quad (52)$$

$$+ E\left\{ \sum_{m=1}^M \sum_{n \neq m}^M \hat{\mathbf{h}}_{q,m}^\dagger \mathbf{g}_{j,m} \mathbf{g}_{j,n}^\dagger \hat{\mathbf{h}}_{q,n} \|\hat{\mathbf{p}}_{j,m}\| \|\hat{\mathbf{p}}_{j,n}\| \Lambda_{1,2_m} \Lambda_{1,2_n} \right\} \quad (53)$$

Now, denote

$$w = \hat{\mathbf{h}}_{q,m}, \mathbf{g}_{j,n}, \hat{\mathbf{h}}_{q,n}, \|\mathbf{h}_{q,m}\|, \|\mathbf{h}_{q,n}\|, \|\hat{\mathbf{p}}_{j,m}\|, \|\hat{\mathbf{p}}_{j,n}\| \quad (54)$$

and using the same independence argument as in (43), the double sum in (53) can be written as

$$\sum_{m=1}^M \sum_{n \neq m}^M E\left\{ E\left\{ \hat{\mathbf{h}}_{q,m}^\dagger \mathbf{g}_{j,m} \mathbf{g}_{j,n}^\dagger \hat{\mathbf{h}}_{q,n} \|\hat{\mathbf{p}}_{j,m}\| \|\hat{\mathbf{p}}_{j,n}\| \left| \bar{\mathbf{p}}_{j,m}, w \right. \right\} \right\} E\left\{ \Lambda_{1,2_m} \Lambda_{1,2_n} \right\} \quad (55)$$

Given w , all the arguments inside the internal expectation are constants, except $\mathbf{g}_{j,m}$. Furthermore, recalling that given $\bar{\mathbf{p}}_{j,m}$, $\mathbf{g}_{j,m}$ is uniformly distributed on the unit sphere of the null space of

$\bar{\mathbf{p}}_{j,m}$, it follows that $\mathbb{E}\{\mathbf{g}_{j,m}|\bar{\mathbf{p}}_{j,m}, w\} = \mathbf{0}_{N_t}$. Thus, the double sum in (53) is equal to zero. Applying the Cauchy-Schwarz inequality to (52) and using the independence argument again as in (43), one obtains

$$E \leq \sum_{m=1}^M \mathbb{E}\{|\hat{\mathbf{h}}_{q,m}^\dagger \mathbf{g}_{j,m}|^2\} \mathbb{E}\{\|\mathbf{h}_{q,m}\|^2\} \mathbb{E}\{\|\hat{\mathbf{p}}_{j,m}\|^2\} \mathbb{E}\{\Lambda_{1,2m}^2\}. \quad (56)$$

Next, from (56),

$$E \leq \frac{\alpha_q N_t}{M} \mathbb{E}\{|\hat{\mathbf{h}}_{q,m}^\dagger \mathbf{g}_{j,m}|^2\} \mathbb{E}\{\cos^2 \theta_{q,m}\} \mathbb{E}\{\sin^2 \phi_{j,m}\} \quad (57)$$

where we used similar arguments as in (48) concerning the angles, and in addition, $\mathbb{E}\{\|\bar{\mathbf{h}}_{q,m}\|^2\}/\alpha_{q,m} = N_t$ [9], $\sum_{m=1}^M \alpha_{q,m} = \alpha_q$, and $\mathbb{E}\{\|\hat{\mathbf{p}}_{j,m}\|^2\} = \frac{1}{M}$.

To further simplify (57), we treat each of the expressions in the r.h.s. separately. First

$$\mathbb{E}\{\cos^2 \theta_{q,m}\} \mathbb{E}\{\sin^2 \phi_{j,m}\} \leq (1 - \mathcal{U}(2^{B/Q}, a)) 2^{\frac{-B}{Q(N_t-1)}} \quad (58)$$

where we used (49) as well as the upper bound [9]

$$\mathbb{E}\{\sin^2 \phi_{j,m}\} \leq 2^{\frac{-B}{Q(N_t-1)}}. \quad (59)$$

Next, consider $\hat{\mathbf{h}}_{q,m} = \mathbf{P}_{\mathbf{g}_{j,m}} \hat{\mathbf{h}}_{q,m} + \mathbf{P}_{\mathbf{g}_{j,m}}^\perp \hat{\mathbf{h}}_{q,m}$, where $\mathbf{P}_{\mathbf{g}_{j,m}}$, $\mathbf{P}_{\mathbf{g}_{j,m}}^\perp$ are the projection matrices into space spanned by $\mathbf{g}_{j,m}$ and its orthogonal complement, respectively. It follows that

$$\begin{aligned} \mathbb{E}\{|\hat{\mathbf{h}}_{q,m}^\dagger \mathbf{g}_{j,m}|^2\} &= \mathbb{E}\{|\left((\mathbf{P}_{\mathbf{g}_{j,m}} \hat{\mathbf{h}}_{q,m})^\dagger + (\mathbf{P}_{\mathbf{g}_{j,m}}^\perp \hat{\mathbf{h}}_{q,m})^\dagger\right) \mathbf{g}_{j,m}|^2\} \\ &\stackrel{(a)}{=} \mathbb{E}\{|\left(\mathbf{P}_{\mathbf{g}_{j,m}} \hat{\mathbf{h}}_{q,m}\right)^\dagger \mathbf{g}_{j,m}|^2\} \stackrel{(b)}{\leq} \mathbb{E}\left\{\left|\frac{(\mathbf{P}_{\mathbf{g}_{j,m}} \hat{\mathbf{h}}_{q,m})^\dagger}{\|\mathbf{P}_{\mathbf{g}_{j,m}} \hat{\mathbf{h}}_{q,m}\|} \mathbf{g}_{j,m}\right|^2\right\} \stackrel{(c)}{=} \frac{1}{N_t - 1} \end{aligned} \quad (60)$$

where (a) follows because $\mathbf{P}_{\mathbf{g}_{j,m}}^\perp \mathbf{g}_{j,m} = \mathbf{0}_{N_t}$ and (b) follows from $\|\mathbf{P}_{\mathbf{g}_{j,m}} \hat{\mathbf{h}}_{q,m}\| \leq 1$ (recall that $\|\hat{\mathbf{h}}_{q,m}\| = 1$). (c) follows because $\mathbf{g}_{j,m}$ is independent of $\mathbf{P}_{\mathbf{g}_{j,m}} \hat{\mathbf{h}}_{q,m}$, and is uniformly distributed on the unit sphere of the $(N_t - 1)$ -dimensional null space of $\bar{\mathbf{p}}_{j,m}$. Thus, the expectation on the left-hand side of (c) is taken according to the $\beta(1, N_t - 2)$ distribution [9].

Substituting (58) and (60) into (57) establishes (51) for E . The proof for F is identical and is omitted here due to space limitations. \blacksquare

Proposition 11: The term G in (40) satisfies $G \leq \frac{\alpha_q N_t}{M(N_t-1)} 2^{-\frac{2B}{Q(N_t-1)}}$.

Proof: Similar to the derivation of (56), it can be shown that

$$G \leq \sum_{m=1}^M \mathbb{E}\{|\mathbf{s}_{q,m}^\dagger \mathbf{g}_{j,m}|^2\} \mathbb{E}\{\|\mathbf{h}_{q,m}\|^2\} \mathbb{E}\{\|\hat{\mathbf{p}}_{j,m}\|^2\} \mathbb{E}\{\Lambda_{2,2m}^2\}. \quad (61)$$

Next, $E\{|s_{q,m}^\dagger \mathbf{g}_{j,m}|^2\}$ can be bounded using similar arguments as in (60), and by further employing (59), one obtains the desired result. ■

Proposition 12: Consider $H = \{\Xi_i\}_{i=1}^{12}$ (cf. (40)), then $\Xi_i = 0, \forall i \in \{1 \dots 12\}$.

Proof: The proposition will be proven only for Ξ_1 , where for the rest $\Xi_i, i > 1$ the proof is identical. Similar to (55), and with $w = \hat{\mathbf{h}}_{q,m}, \bar{\mathbf{p}}_{j,m}, \hat{\mathbf{h}}_{q,n}, \|\mathbf{h}_{q,m}\|, \|\mathbf{h}_{q,n}\|, \|\hat{\mathbf{p}}_{j,m}\|, \|\hat{\mathbf{p}}_{j,n}\|$ it can be shown that $E\{\mathbf{g}_{j,n}^\dagger | \bar{\mathbf{p}}_{j,n}, w\} = \mathbf{0}_{N_t}$. Thus, $\Xi_1 = 0$, which establishes the desired result. ■

To complete the proof, we apply Propositions 9 to 12 on (40), and in turn, substitute the result in (38), which establishes the desired result.

APPENDIX B

To prove Lemma 3, we begin by bounding A_2 (cf. (19)). Let $\theta_q = \angle\langle \bar{\mathbf{h}}_q, \hat{\mathbf{h}}_q \rangle$ where $\bar{\mathbf{h}}_q = \mathbf{h}_q / \|\mathbf{h}_q\|$ (cf. (2)), $\hat{\mathbf{h}}_q = \hat{\mathbf{h}}_q / \|\hat{\mathbf{h}}_q\|$ (cf. (5)) and $\xi_q = \angle\langle \hat{\mathbf{h}}_q, \hat{\mathbf{p}}_q \rangle$. Since the argument of the logarithm in A_2 is always positive; i.e., $|\bar{\mathbf{h}}_q^\dagger \hat{\mathbf{p}}_q| > 0$, we assume without loss of generality that $\angle\langle \bar{\mathbf{h}}_q, \hat{\mathbf{p}}_q \rangle \in [0, \pi/2]$. Employing the triangle inequality for angles, one obtains,

$$\angle\langle \bar{\mathbf{h}}_q, \hat{\mathbf{p}}_q \rangle \leq \theta_q + \xi_q \quad (62)$$

Applying $\cos^2(\cdot)$ on both sides is possible if $0 \leq \xi_q + \theta_q \leq \frac{\pi}{2}$, which guarantees the monotonicity of the cosine. Denote the common probability space, in which all random variables we are dealing with are defined, by $(\Omega, \mathcal{F}, \mathbb{P})$, and let

$$\mathcal{A}_q = \left\{ \omega \in \Omega : 0 \leq \xi_q(\omega) + \theta_q(\omega) \leq \frac{\pi}{2} \right\}. \quad (63)$$

Furthermore, for X , a random variable defined on $(\Omega, \mathcal{F}, \mathbb{P})$ and for $\mathcal{A} \in \mathcal{F}$, we denote the random variable $\chi_{\mathcal{A}}(\omega)X(\omega)$ by $\chi_{\mathcal{A}}X$. Combining (63) and (62), it follows that

$$|\bar{\mathbf{h}}_q^\dagger \hat{\mathbf{p}}_q|^2 = \cos^2(\angle\langle \bar{\mathbf{h}}_q, \hat{\mathbf{p}}_q \rangle) \geq \chi_{\mathcal{A}_q} \cos^2(\angle\langle \bar{\mathbf{h}}_q, \hat{\mathbf{p}}_q \rangle) \geq \chi_{\mathcal{A}_q} \cos^2(\xi_q + \theta_q) \quad (64)$$

and from the definition of A_2 (cf. (19)) and the monotonicity of $\log(1+x)$, it follows that

$$A_2 \geq E\left\{ \chi_{\mathcal{A}_q} \log(1 + P\|\mathbf{h}_q\|^2 \cos^2(\xi_q + \theta_q)) \right\}. \quad (65)$$

Proposition 13: Let $K(x) \triangleq \frac{\pi x}{2\sqrt{x+1}}$, then

$$\log(1 + P\|\mathbf{h}_q\|^2 \cos^2(\xi_q + \theta_q)) \geq \log(1 + P\|\mathbf{h}_q\|^2 \cos^2(\xi_q)) - \sin(\theta_q)K(P\|\mathbf{h}_q\|^2). \quad (66)$$

Proof: Let $\check{P} = P\|\mathbf{h}_q\|^2$ and $g(\theta, \xi) \triangleq \log(1 + \check{P} \cos^2(\theta + \xi))$ for $\theta, \xi \in [0, \pi/2]$, where for brevity we omit the subscript q in this proof. To bound $g(\theta, \xi)$, we solve $g^{(2,0)}(\theta, \xi) = 0$, from which the inflection point is given by $\theta_1 = \cos^{-1}((1/\check{P} + 2)^{1/2}) - \xi$ and $g^{(1,0)}(\theta_1, \xi) = -\check{P}(\check{P} + 1)^{-1/2}$. Furthermore, it can be shown that $g(\theta, \xi)$ is convex for $\theta > \theta_1$ and concave otherwise. We first derive a bound for the case where $\theta_1 \leq 0$, in which $g(\theta, \xi)$ is convex for $\theta \in [0, \pi/2]$ and therefore, $g(\theta, \xi) \geq \theta g^{(1,0)}(0, \xi) + g(0, \xi)$. Moreover, it can be shown that $g^{(1,0)}(\theta, \xi) < 0, \forall \theta + \xi < \frac{\pi}{2}$. Then, using $\frac{\pi}{2} \sin(\theta) > \theta$ we replace θ with $\frac{\pi}{2} \sin(\theta)$ and obtain $g(\theta, \xi) \geq \frac{\pi}{2} \sin(\theta) g^{(1,0)}(0, \xi) + g(0, \xi)$. Noting that $g^{(1,0)}(0, \xi) = -\frac{2\check{P} \sin(\xi) \cos(\xi)}{\check{P} \cos^2(\xi) + 1} \geq -\check{P}(\check{P} + 1)^{-1/2}$ and substituting $g(0, \xi)$ into the latter inequality, we obtain (66), which establishes the result for $\theta_1 \leq 0$. In the case where $\theta_1 > 0$, we use the Lipschitz continuity; i.e., a function $f(x)$ is Lipschitz continuous if $\exists C > 0$ such that $|f(x_1) - f(x_2)| \leq C|x_1 - x_2| \forall x_1, x_2$. If $f(x)$ is differentiable, then $C = \sup_x |df(x)/dx|$. Since $g(\theta, \xi)$ is Lipschitz continuous, by replacing C with the inflection point, one obtains $g(\theta, \xi) \geq g(0, \xi) + \frac{\pi}{2} \sin(\theta) g^{(1,0)}(\theta_1, \xi) = \log(1 + \check{P} \cos^2(\xi)) - \sin(\theta) K(\check{P})$. Finally, because the bounds for $\theta_1 \leq 0$ and $\theta_1 > 0$ are identical, the desired result follows. ■

Substituting (66) into (65), it follows that

$$A_2 \geq E_2 - \mathbf{E}\{\chi_{\mathcal{A}_q} \sin(\theta_q) K(P\|\mathbf{h}_q\|^2)\} \quad (67)$$

where $E_2 = \mathbf{E}\{\chi_{\mathcal{A}_q} \log(1 + P\|\mathbf{h}_q\|^2 \cos^2 \xi_q)\}$, and by Cauchy–Schwarz and Jensen’s inequality (K is concave) it follows $A_2 \geq E_2 - \mathbf{E}\{\chi_{\mathcal{A}_q}\} \mathbf{E}\{\sin(\theta_q)\} K(P\mathbf{E}\{\|\mathbf{h}_q\|^2\})$. Hence

$$A_2 \geq E_2 - \mathbf{E}\{\chi_{\mathcal{A}_q}\} \mathbf{E}\{\sqrt{Z_q}\} \frac{\pi \alpha_q P N_t}{2\sqrt{\alpha_q P N_t + 1}} \quad (68)$$

where we substituted $\sin(\theta_q) = \sqrt{Z_q}$. To bound the term E_2 (cf. (67)) we invoke, once again, the triangular inequality for angles, $\xi_q \leq \phi_q + \angle\langle \hat{\mathbf{h}}_q, \mathbf{p}_q \rangle$, where $\phi_q = \angle\langle \mathbf{p}_q, \hat{\mathbf{p}}_q \rangle$, and obtain

$$E_2 \geq \mathbf{E}\left\{\chi_{\mathcal{C}_q} \log\left(1 + P\|\mathbf{h}_q\|^2 \cos^2(\angle\langle \hat{\mathbf{h}}_q, \mathbf{p}_q \rangle + \phi_q)\right)\right\} \quad (69)$$

where $\mathcal{C}_q = \mathcal{A}_q \cap \mathcal{B}_q$ and $\mathcal{B}_q = \{\omega \in \Omega : 0 \leq \angle\langle \hat{\mathbf{h}}_q, \mathbf{p}_q \rangle(\omega) + \phi_q(\omega) \leq \frac{\pi}{2}\}$. Using similar arguments as in (66)-(68), it can be shown that

$$E_2 \geq \mathbf{E}\left\{\chi_{\mathcal{C}_q} \log\left(1 + P\|\mathbf{h}_q\|^2 \cos^2(\angle\langle \hat{\mathbf{h}}_q, \mathbf{p}_q \rangle)\right)\right\} - \mathbf{E}\{\chi_{\mathcal{C}_q}\} \mathbf{E}\{\sin(\phi_q)\} \frac{\pi \alpha_q P N_t}{2\sqrt{\alpha_q P N_t + 1}} \quad (70)$$

Before continuing, the following proposition is necessary.

Proposition 14: Let $Z_q = \sin^2(\theta_q)$. Then, $Z_q^{\min} \leq Z_q \leq Z_q^{\max}$, where $Z_q^{\min} = \min\{Z_{q,l}, l \in \mathcal{M}\}$ and $Z_q^{\max} = \max\{Z_{q,l}, l \in \mathcal{M}\}$. Moreover, $\mathcal{U}(2^{B/Q}, a/2) - \mathcal{V}_M(2^{B/Q}, a/2) \leq \mathbb{E}\{\sqrt{Z_q}\} \leq \mathcal{U}(2^{B/Q}, a/2) + \mathcal{V}_M(2^{B/Q}, a/2)$ where $\mathcal{U}(\cdot)$ and $\mathcal{V}_M(\cdot)$ defined in (16) and (17), respectively.

Proof: Consider $Z_q = 1 - \frac{|\hat{\mathbf{h}}_q^\dagger \mathbf{h}_q|^2}{\|\mathbf{h}_q\|^2 \|\hat{\mathbf{h}}_q\|^2} = \sum_{u=1}^M \sum_{l=1}^M \frac{\|\mathbf{h}_{q,l}\|^2 \|\hat{\mathbf{h}}_{q,u}\|^2}{\|\mathbf{h}_q\|^2 \|\hat{\mathbf{h}}_q\|^2} \left(1 - \sqrt{1 - Z_{q,l}} \sqrt{1 - Z_{q,u}}\right)$ where we used (2), (5) and (7). Thus,

$$Z_q \leq \frac{1}{\|\mathbf{h}_q\|^2 \|\hat{\mathbf{h}}_q\|^2} \sum_{u=1}^M \sum_{l=1}^M \|\mathbf{h}_{q,l}\|^2 \|\hat{\mathbf{h}}_{q,u}\|^2 \left(1 - (\min\{\sqrt{1 - Z_{q,l}}, l \in \mathcal{M}\})^2\right) = Z_q^{\max}$$

Similarly, it can be shown that $Z_q \geq Z_q^{\min}$, which establishes the first statement of the theorem.

The bound on $\mathbb{E}\{\sqrt{Z_q}\}$ follows from the identities, $\mathbb{E}\{Z_q^{\max}\} \leq \mathbb{E}\{Z_{q,l}\} + \frac{(M-1)\sqrt{\text{var}\{Z_{q,l}\}}}{\sqrt{2M-1}}$, $\mathbb{E}\{Z_q^{\min}\} \geq \mathbb{E}\{Z_{q,l}\} - \frac{(M-1)\sqrt{\text{var}\{Z_{q,l}\}}}{\sqrt{2M-1}}$ (cf. [37], Sec. 4.2). ■

Note that $\sin(\theta_q)$ and $\sin(\phi_q)$ are identically distributed; therefore, the expression in Proposition 14 also applies to $\sin(\phi_q)$.

Returning to the main proof; by invoking Proposition 14 and combining the latter with (68) and (70), one obtains $A_2 \geq \mathbb{E}\{\chi_{C_q} \log(1 + P|\hat{\mathbf{h}}_q^\dagger \mathbf{p}_q|^2)\} - (\mathbb{E}\{\chi_{\mathcal{A}_q}\} + \mathbb{E}\{\chi_{C_q}\}) \frac{\pi \alpha_q P N_t}{2\sqrt{\alpha_q P N_t + 1}} [\mathcal{U}(2^{B/Q}, a/2) + \mathcal{V}_M(2^{B/Q}, a/2)]$. It, therefore, follows that

$$A_1 - A_2 \leq \mathbb{E}\{(1 - \chi_{C_q})\} \mathbb{E}\{\log(1 + P|\hat{\mathbf{h}}_q^\dagger \mathbf{p}_q|^2)\} \quad (71)$$

$$+ \frac{\pi \alpha_q P N_t}{\sqrt{\alpha_q P N_t + 1}} [\mathcal{U}(2^{B/Q}, a/2) + \mathcal{V}_M(2^{B/Q}, a/2)] \quad (72)$$

wherein (71) we used the fact that $|\hat{\mathbf{h}}_q^\dagger \mathbf{p}_q|^2$ and $|\mathbf{h}_q^\dagger \mathbf{p}_q^*|^2$ are identically distributed and the Cauchy-Schwarz inequality and in (72) we used $0 \leq \mathbb{E}\{\chi_{\mathcal{A}_q}\}, \mathbb{E}\{\chi_{C_q}\} \leq 1$.

It remains to bound $\mathbb{E}\{1 - \chi_{C_q}\}$; i.e., $\mathbb{P}(\mathcal{C}_q^c)$ (cf. (69)), where $\mathbb{P}(\cdot)$ is the probability measure.

Beginning with $\mathbb{P}(\mathcal{A}_q^c)$, we derive a bound on $\cos^2(\xi_q)$. Consider, $\hat{\mathbf{p}}_q = \cos(\phi_q) \mathbf{p}_q + \sin(\phi_q) \mathbf{g}_q$, and note that \mathbf{p}_q (cf. (6)) can be seen as the projection of $\hat{\mathbf{h}}_q$ into the orthogonal complement of $\mathcal{H}_{-q} = \text{span}(\hat{\mathbf{h}}_1, \dots, \hat{\mathbf{h}}_{q-1}, \hat{\mathbf{h}}_{q+1}, \dots, \hat{\mathbf{h}}_Q)$; after being normalized; that is, $\mathbf{p}_q = \frac{\mathbf{P}_{\mathcal{H}_{-q}}^\perp \hat{\mathbf{h}}_q}{\|\mathbf{P}_{\mathcal{H}_{-q}}^\perp \hat{\mathbf{h}}_q\|}$. We

further express $\hat{\mathbf{h}}_q$ as $\hat{\mathbf{h}}_q = V_1 \mathbf{p}_q + V_2 \frac{\mathbf{P}_{\mathcal{H}_{-q}} \hat{\mathbf{h}}_q}{\|\mathbf{P}_{\mathcal{H}_{-q}} \hat{\mathbf{h}}_q\|}$, where $V_1 \sim \Gamma(N_t - Q + 1, 1)$, $V_2 \sim \Gamma(Q - 1, 1)$ and denote $W_q = \cos^2(\angle(\hat{\mathbf{h}}_q, \mathbf{p}_q))$. It, therefore, follows that $\sqrt{W_q} = \frac{V_2}{\sqrt{V_1^2 + V_2^2}} \sim \beta(MN_t - Q + 1, Q - 1)$ [38]. Combining the latter representations of $\hat{\mathbf{p}}_q$ and $\hat{\mathbf{h}}_q$, one obtains $\cos^2(\xi_q) = |\hat{\mathbf{h}}_q^\dagger \hat{\mathbf{p}}_q|^2 = |\sin(\phi_q) \hat{\mathbf{h}}_q^\dagger \mathbf{g}_q + \cos(\phi_q) \hat{\mathbf{h}}_q^\dagger \mathbf{p}_q|^2 \geq -|\sin(\phi_q) \hat{\mathbf{h}}_q^\dagger \mathbf{g}_q|^2 + |\cos(\phi_q) \sqrt{W_q}|^2 \geq \cos^2(\phi_q) W_q - \sin^2(\phi_q)$

Now to $\mathbb{P}(\mathcal{A}_q)$. Consider $\mathbb{P}(\mathcal{A}_q^c) = \mathbb{P}(\xi_q > \frac{\pi}{2} - \theta_q) = \mathbb{P}(\cos^2(\xi_q) \leq \sin^2(\theta_q))$, then $\mathbb{P}(\mathcal{A}_q^c) \leq \mathbb{P}(\cos^2(\phi_q) W_q - \sin^2(\phi_q) \leq \sin^2(\theta_q)) \leq \mathbb{P}(W_q \leq \sin^2(\theta_q) + 2\sin^2(\phi_q))$, wherein the latter

we used $\cos^2(\phi_q) = 1 - \sin^2(\phi_q)$ and $0 \leq W_q \leq 1$. Let $Y_q = \sin^2(\theta_q) + 2\sin^2(\phi_q)$ and let $F_{Y_q[y]} = \mathbb{P}(Y_q \leq y)$, then, $\mathbb{P}(\mathcal{A}_q^c) \leq \mathbb{P}(W_q \leq Y_q) = \int \mathbb{P}(W_q \leq y | Y_q = y) dF_{Y_q}(y) = \mathbb{E}\{\mathbb{P}(W_q \leq y | Y_q = y)\}$. Since W_q is independent of θ_q and ϕ_q , $\mathbb{P}(W_q \leq y | Y_q = y) = I_y(MN_t - Q + 1, Q - 1)$ where I_y is the regularized beta function. Using $I_y(MN_t - Q + 1, Q - 1) \leq y$ for $0 \leq y \leq 1$, one obtains $\mathbb{P}(\mathcal{A}_q^c) \leq \mathbb{E}\{Y_q\} = \mathbb{E}\{\sin^2(\theta_q) + 2\sin^2(\phi_q)\}$. Next, similar to Proposition 14, it can be shown that $\mathbb{P}(\mathcal{A}_q^c) \leq 3(\mathcal{U}(2^{B/Q}, a) + \mathcal{V}_M(2^{B/Q}, a))$, where a, \mathcal{U} and \mathcal{V}_M are defined in Theorem 1. To complete the proof, we bound $\mathbb{P}(\mathcal{C}_q^c)$ as follows $\mathbb{P}(\mathcal{C}_q^c) = \mathbb{P}((\mathcal{A}_q \cup \mathcal{B}_q)^c) \leq \mathbb{P}(\mathcal{A}_q^c \cup \mathcal{B}_q^c) \leq \mathbb{P}(\mathcal{A}_q^c) + \mathbb{P}(\mathcal{B}_q^c)$. Finally, similar to $\mathbb{P}(\mathcal{A}_q^c)$, it can be shown that $\mathbb{P}(\mathcal{B}_q^c) \leq 3(\mathcal{U}(2^{B/Q}, a) + \mathcal{V}_M(2^{B/Q}, a))$, which establishes the desired result.

APPENDIX C

The proof of Lemma 6 is similar to the proof of Lemma 2 (cf. Appendix A). It is obtained by substituting $\tilde{\mathbf{h}}_q, \hat{\mathbf{h}}_q, \tilde{\mathbf{p}}_j, \hat{\mathbf{p}}_j, \tilde{\mathbf{s}}_{q,m}, \tilde{\mathbf{g}}_{j,m}, \tilde{P}, B/(Q - \bar{Q})$ for $\mathbf{h}_q, \hat{\mathbf{h}}_q, \mathbf{p}_j, \hat{\mathbf{p}}_j, \mathbf{s}_{q,m}, \mathbf{g}_{j,m}, P, B/Q$, respectively. Moreover, because $\mathbb{E}\{\|\hat{\mathbf{h}}_{q,m}\|^2\}/\alpha_{q,m} = \tilde{N}_t$ [9], N_t, a are replaced by \tilde{N}_t, \tilde{a} , respectively, and $\alpha_{q,m}$ by $1/M$, due to Assumption 8. The desired result then follows similarly with few caveats as follows.

The sums in (39), (40), (43)-(46), (52), (56), (61) now run over $\mathcal{M}_{q,j}$, (cf. Definition 4), rather than \mathcal{M} ; that is, $\sum_{m=1}^M(\cdot)$ is replaced with $\sum_{m \in \mathcal{M}_{q,j}}(\cdot)$. Similarly, the double sums in (41), (43), (45), (53), (55) now run over $m, n \in \mathcal{M}_{q,j}$. Furthermore, because $\mathbb{E}\{\|\tilde{\mathbf{p}}_{j,m}\|^2\} = \frac{1}{M_j}$, the term M in (47), (57) is now changed to M_j . These modifications, and Assumption 8 imply that $\sum_{m \in \mathcal{M}_{q,j}} \alpha_{q,m} = M_{q,j}/M$, which thus affect Propositions 9 to 11 in which α_q/M is replaced with $M_{q,j}/M_j M$.

Now to $\tilde{A}_1 - \tilde{A}_2 \leq \Delta \tilde{R}_{2,q}$; the proof is similar to that of Lemma 3 (cf. Appendix B). It is obtained by substituting $\tilde{\mathbf{h}}_q, \hat{\mathbf{h}}_q, \tilde{\mathbf{p}}_j, \hat{\mathbf{p}}_j, M_q, \tilde{P}, \tilde{N}_t, \tilde{a}, B/(Q - \bar{Q})$ for $\mathbf{h}_q, \hat{\mathbf{h}}_q, \mathbf{p}_j, \hat{\mathbf{p}}_j, M, P, N_t, a, B/Q$, respectively, in Appendix B, and following similar steps.

REFERENCES

- [1] A. Checko, H. L. Christiansen, Y. Yan, L. Scolari, G. Kardaras, M. S. Berger, and L. Dittmann, "Cloud RAN for mobile networks - a technology overview," *IEEE Commun. Surveys & Tutorials*, vol. 17, no. 1, pp. 405–426, 2015.
- [2] B. Dai and W. Yu, "Sparse beamforming for limited-backhaul network MIMO system via reweighted power minimization," in *Global Commun. Conf. (GLOBECOM), 2013 IEEE*, pp. 1962–1967, IEEE, 2013.

- [3] R. Zakhour and D. Gesbert, “Optimized data sharing in multicell MIMO with finite backhaul capacity,” *IEEE Trans. Signal Process.*, vol. 59, no. 12, pp. 6102–6111, 2011.
- [4] L. M. Larsen, A. Checko, and H. L. Christiansen, “A survey of the functional splits proposed for 5G mobile crosshaul networks,” *IEEE Commun. Surv. Tutorials*, vol. 21, no. 1, pp. 146–172, 2019.
- [5] P. De Kerret and D. Gesbert, “CSI sharing strategies for transmitter cooperation in wireless networks,” *IEEE Wireless Communications*, vol. 20, pp. 43–49, February 2013.
- [6] P. De Kerret, J. Hoydis, and D. Gesbert, “Rate loss analysis of transmitter cooperation with distributed CSIT,” in *IEEE Work. Signal Process. Adv. Wirel. Commun. SPAWC*, pp. 190–194, IEEE, 2013.
- [7] Q. Li, P. de Kerret, D. Gesbert, and N. Gresset, “Robust regularized ZF in cooperative broadcast channel under distributed (CSIT),” *IEEE Trans. Inf. Theory*, vol. 66, no. 3, pp. 1845–1860, 2020.
- [8] P. De Kerret and D. Gesbert, “Spatial CSIT allocation policies for network MIMO channels,” *IEEE Trans. Inf. Theory*, vol. 60, no. 7, pp. 4158–4169, 2014.
- [9] N. Jindal, “MIMO broadcast channels with finite-rate feedback,” *IEEE Trans. Inf. Theory*, vol. 52, pp. 5045–5060, Nov 2006.
- [10] G. Caire, N. Jindal, M. Kobayashi, and N. Ravindran, “Multiuser MIMO achievable rates with downlink training and channel state feedback,” *IEEE Trans. Inf. Theory*, vol. 56, June 2010.
- [11] B. Makki, J. Li, T. Eriksson, and T. Svensson, “Throughput analysis for multi-point joint transmission with quantized CSI feedback,” in *Veh. Technol. Conf. (VTC Fall), 2012 IEEE*, pp. 1–5, IEEE, 2012.
- [12] S. Yu, H.-B. Kong, Y.-T. Kim, S.-H. Park, and I. Lee, “Novel feedback bit allocation methods for multi-cell joint processing systems,” *IEEE Trans. Wireless Commun.*, vol. 11, no. 9, pp. 3030–3036, 2012.
- [13] D. Jaramillo-Ramirez, M. Kountouris, and E. Hardouin, “Coordinated multi-point transmission with imperfect CSI and other-cell interference,” *IEEE Trans. Wireless Commun.*, vol. 14, no. 4, pp. 1882–1896, 2015.
- [14] J. Zhang, C. K. Wen, S. Jin, X. Gao, and K. K. Wong, “Large system analysis of cooperative multi-cell downlink transmission via regularized channel inversion with imperfect CSIT,” *IEEE Trans. Wirel. Commun.*, vol. 12, pp. 4801–4813, oct 2013.
- [15] L. Sanguinetti, R. Couillet, and M. Debbah, “Large system analysis of base station cooperation for power minimization,” *IEEE Trans. Wirel. Commun.*, vol. 15, no. 8, pp. 5480–5496, 2016.
- [16] J. Li, D. Wang, P. Zhu, J. Wang, and X. You, “Downlink spectral efficiency of distributed massive MIMO systems with linear beamforming under pilot contamination,” *IEEE Trans. Veh. Technol.*, vol. 67, no. 2, pp. 1130–1145, 2018.
- [17] C. Pan, H. Zhu, N. J. Gomes, and J. Wang, “Joint precoding and RRH selection for user-centric green MIMO C-RAN,” *IEEE Trans. Wirel. Commun.*, vol. 16, no. 5, pp. 2891–2906, 2017.
- [18] C. Pan, M. ElKashlan, J. Wang, J. Yuan, and L. Hanzo, “User-centric C-RAN architecture for ultra-dense 5G networks: Challenges and methodologies,” *IEEE Commun. Mag.*, vol. 56, pp. 14–20, jun 2018.
- [19] C. Pan, H. Ren, M. ElKashlan, A. Nallanathan, and L. Hanzo, “Robust beamforming design for ultra-dense

- user-centric C-RAN in the face of realistic pilot contamination and limited feedback,” *IEEE Trans. Wirel. Commun.*, vol. 18, pp. 780–795, Feb 2019.
- [20] W. Santipach and M. L. Honig, “Signature optimization for CDMA with limited feedback,” *IEEE Trans. Inf. Theory*, vol. 51, no. 10, pp. 3475–3492, 2005.
- [21] J. Li, D. Wang, P. Zhu, and X. You, “Impacts of practical channel impairments on the downlink spectral efficiency of large-scale distributed antenna systems,” *Sci. China Inf. Sci.*, vol. 62, no. 2, pp. 1–14, 2019.
- [22] M. Wang, D. W. Yue, and S. N. Jin, “Downlink transmission of multicell distributed massive MIMO with pilot contamination under rician fading,” *IEEE Access*, vol. 8, pp. 131835–131847, 2020.
- [23] J. Kang, O. Simeone, J. Kang, and S. S. Shitz, “Joint signal and channel state information compression for the backhaul of uplink network MIMO systems,” *IEEE Trans. Wireless Commun.*, vol. 13, 2014.
- [24] D. Wang, Y. Wang, R. Sun, and X. Zhang, “Robust C-RAN precoder design for wireless fronthaul with imperfect channel state information,” in *Wireless Commun. Netw. Conf. (WCNC)*, pp. 1–6, IEEE, 2017.
- [25] T. R. Lakshmana, A. Tölli, R. Devassy, and T. Svensson, “Precoder design with incomplete feedback for joint transmission,” *IEEE Trans. Wireless Commun.*, vol. 15, no. 3, pp. 1923–1936, 2016.
- [26] Y. Shi, J. Zhang, and K. B. Letaief, “CSI overhead reduction with stochastic beamforming for cloud radio access networks,” in *IEEE Int. Conf. Commun. (ICC)*, pp. 5154–5159, IEEE, 2014.
- [27] D. Tse and P. Viswanath, *Fundamentals of wireless communication*. Cambridge university press, 2005.
- [28] X. Yu, W. Xu, S. H. Leung, Q. Shi, and J. Chu, “Power allocation for energy efficient optimization of distributed MIMO system with beamforming,” *IEEE Trans. Veh. Technol.*, vol. 68, pp. 8966–8981, 2019.
- [29] D. A. Basnayaka, P. J. Smith, and P. A. Martin, “Ergodic sum capacity of macrodiversity MIMO systems,” *IEEE Trans. Inf. Theory*, vol. 59, no. 9, 2013.
- [30] D. A. Basnayaka, P. J. Smith, and P. A. Martin, “Performance analysis of dual-user macrodiversity MIMO systems with linear receivers in flat Rayleigh fading,” *IEEE Trans. Wirel. Commun.*, vol. 11, no. 12, 2012.
- [31] D. A. Basnayaka, P. J. Smith, and P. A. Martin, “Performance analysis of macrodiversity MIMO systems with MMSE and ZF receivers in flat rayleigh fading,” *IEEE Trans. Wirel. Commun.*, vol. 12, 2013.
- [32] R. Senanayake, P. L. Yeoh, and J. Evans, “On the sum capacity of cluster-based cooperative cellular networks,” in *IEEE Int. Conf. Commun.*, pp. 1613–1618, sep 2015.
- [33] Y. Noam and B. M. Zaidel, “On the two-user MISO interference channel with single-user decoding: Impact of imperfect CSIT and channel dimension reduction,” *IEEE Trans. Signal Process.*, vol. 67, no. 10, 2019.
- [34] N. Arad and Y. Noam, “C-RAN zero-forcing with imperfect CSI: Analysis and precoder&quantize feedback,” *arXiv:2012.12551*, 2020.
- [35] 3GPP TR 36.814, *E-UTRA; Further advancements for E-UTRA physical layer aspects*, 3 2010. V9. page 61.
- [36] N. Ravindran and N. Jindal, “Limited feedback-based block diagonalization for the MIMO broadcast channel,” *IEEE Journal on Selected Areas in Communications*, vol. 26, pp. 1473–1482, October 2008.
- [37] A. H. David and H. N. Nagaraja, *Order Statistics*. N. J.: John Wiley, third ed., 2003.

- [38] J. C. Roh and B. D. Rao, "Transmit beamforming in multiple-antenna systems with finite rate feedback: a VQ-based approach," *IEEE Trans. Inf. Theory*, vol. 52, no. 3, pp. 1101–1112, 2006.

SUPPLEMENTARY MATERIAL

A PROOF OF COROLLARY 7

We first show with showing that

$$M_q = (1 - \bar{Q}/Q)M, \forall q \in \mathcal{Q} \quad (\text{S.1})$$

and

$$\sum_{j \in \mathcal{Q}_{-q}} \frac{M_{q,j}}{M_j} = (Q - \bar{Q} - 1). \quad (\text{S.2})$$

Define $L \triangleq Q/M \in \mathbb{N}$, $r \triangleq \bar{Q}/Q$ and note that $rM \in \mathbb{N}$. Without loss of generality, consider $q = 1$ and assume that $\mathcal{Q}_m = \{(m-1)L+1, \dots, mL\}$ for $m \in \mathcal{M}$. From Definition 7, MS-1 is not served by S-RRH-1, ... S-RRH- Mr , therefore $M_1 = M(1-r)$ which establishes (S.1). To show (S.2), we note that $\forall j \in \mathcal{Q}_1$, MS- j is served by the same set of S-RRHs as MS-1; thus, $M_{1,j} = M_1$, $\forall j \in \mathcal{Q}_1$. Assume, for now, that $0 \leq r \leq \frac{1}{2}$; then by the symmetric selection policy $M_{1,j} = M_1 - k \ \forall j \in \{\mathcal{Q}_{(1+k) \bmod M} \cup \mathcal{Q}_{(1-k) \bmod M} : k = 1, \dots, Mr\}$ and $M_{1,j} = M_1 - Mr \ \forall j \in \{\mathcal{Q}_{(k \bmod M)+1} \cup \mathcal{Q}_{(-k \bmod M)+1} : k = Mr+1, \dots, \lfloor M/2 \rfloor\}$. Thus

$$\sum_{i=2}^Q M_{1,i} = (L-1)M_1 + L[(M-2Mr-1)(M_1-Mr) + Mr(-Mr+2M_1-1)]. \quad (\text{S.3})$$

Now to the case where $r > \frac{1}{2}$. Here $M_{1,j} = M_1$, $\forall j \in \mathcal{Q}_1$,

$$M_{1,j} = M_1 - k \ \forall j \in \{\mathcal{Q}_{(k \bmod M)+1} \cup \mathcal{Q}_{(-k \bmod M)+1} : k = 1, \dots, M_1-1\} \quad (\text{S.4})$$

and $M_{1,j} = 0$ otherwise. Thus,

$$\sum_{i=1}^Q M_{1,i} = (L-1)M_1 + L(M_1-1)M_1. \quad (\text{S.5})$$

Substituting $L = Q/M$, $M_1 = M(1-r)$ and $r = \bar{Q}/Q$ in both (S.3), (S.5) it follows that the two expressions are identical and are given by

$$\sum_{i=2}^Q M_{1,i} = \frac{M(Q - \bar{Q} - 1)(Q - \bar{Q})}{Q} \quad (\text{S.6})$$

which establishes (S.1) and (S.2). It remains to calculate $\tilde{T}_q = M_q \tilde{N}_t - \tilde{Q}_q + 1$. Recalling that $M_q = M(1-r)$, it is sufficient to calculate \tilde{Q}_q , which is given by

$$\tilde{Q}_q = Q - \sum_{j \in \mathcal{Q}_{-q}} \chi_{\{0\}}(M_{q,j}) \quad (\text{S.7})$$

Note that $\sum_{j \in \mathcal{Q}-q} \chi_{\{0\}}(M_{q,j})$ can be written as $|\{j, |\mathcal{M}_{q,j}| = 0, j \neq q\}|$; i.e., the number of MSs served by at least one S-RRH that serves MS- q . For $r \geq \frac{1}{2}$, the latter sum is equal to $2Q(1 - r) - L - 1$, whereas for $r < 1/2$, $\tilde{Q}_q = Q - 1$. This can be written as, $\tilde{Q}_q = Q - \min(Q, -2\bar{Q} + (2 - 1/M)Q - 1)$, and therefore

$$\tilde{T}_q = M(1 - r)\tilde{N}_t + 1 - \min \left[Q, \left(2 - \frac{1}{M} \right) Q - 2\bar{Q} \right] \quad (\text{S.8})$$

which establishes the desired result.

B A DETAILED DESCRIPTION OF THE SIMULATION SETUP

We now provide a detailed description of the two simulation setups considered in Fig. 3. Here we consider a practically oriented setup with randomly dispersed MSs while considering propagation loss and shadowing. The setup includes a cluster of $M = 4$ S-RRHs, each placed at the center of one of four adjacent hexagons, creating a hexagonal grid with an edge-length of 100 m; i.e., we cut four hexagons and placed an S-RRH at the center of each hexagon. Each S-RRH is equipped with $N_t = 8$ isotropic transmit antennas. Eight single-antenna MSs ($Q = 8$) were placed uniformly at random in the area spanned by the hexagons, with a minimum distance of 10 m between each MS and S-RRH. The results were averaged over 20 realizations of MS-placements, where each realization determined a set of attenuation factors $\alpha = \{\alpha_{q,m} : q = 1 \cdots 8, m = 1 \cdots 4\}$ according $\alpha_{q,m} = -128 - 37.6 \log_{10}(r_{q,m})$ (in dB),²¹ where $r_{q,m}$ is the distance from S-RRH- m to MS- q in Km. The noise level at the receivers was -121 dBm. For each realization α , we calculated the rates $\hat{R}_q(\alpha)$, $\hat{\hat{R}}_q(\alpha)$ using (10) and Definition 5, for the corresponding scheme,²² by averaging over 40 realizations of $\{\mathbf{h}_{q,m}\}_{q \in \mathcal{Q}, m \in \mathcal{M}}$, generated according to Assumption 1. The network throughput for a given α was calculated as $\bar{R}(\alpha) = 1/Q \sum_{q=1}^Q \hat{R}_q(\alpha)$, and the throughput \bar{R} was calculated by averaging $\bar{R}(\alpha)$ over 20 realizations of α ; i.e., $\bar{R} = 1/20 \sum_{i=1}^{20} \bar{R}(\alpha_i)$, where each α_i corresponded to a different MS placement. $\tilde{\bar{R}}(\alpha)$ and $\tilde{\bar{R}}$ are defined similarly.

To ensure a fair comparison, in all figures (Figures 3(a) and 3(b)) we considered that the transmitters could always turn off some of their antennas to reduce the effective MISO channel dimensions. Therefore, in the standard scheme, for each α , we evaluated $\bar{R}(\alpha)$ for $N_t = \{2, \dots, 8\}$

²¹This model was used for urban-area non-line-of-site links by the 3GPP; cf. page 61 3GPP Technical Report 36.814 [35].

²² $\hat{R}_q(\alpha)$ is a function of α by (9) and by Assumption 1.

and picked the maximum. We applied a similar procedure for the P&Q scheme, where we maximized the rate over \bar{Q} , with $N_t = 8$; i.e., by evaluating $\bar{R}(\boldsymbol{\alpha})$ for $\bar{Q} = \{1, \dots, 6\}$ and taking the maximum.

Finally, we used the following power allocation strategy.

Definition 8 (The equal power-backoff strategy): Considering the standard feedback scheme, each S-RRH transmits with equal power to each MS; i.e., $P_{q,m} = P, \forall q \in \mathcal{Q}, m \in \mathcal{M}$. To avoid violating its individual power constraint P_{\max} , each S-RRH sets $P = \frac{\gamma P_{\max}}{Q}$, where $\gamma \geq 1$ is the backoff factor, given by

$$\gamma = \min \left\{ \gamma_m : \sum_{q \in \mathcal{Q}} \gamma_m \|\mathbf{p}_{q,m}\|^2 = Q, m \in \mathcal{M} \right\} \quad (\text{S.9})$$

To explain this strategy, we note that $\mathbb{E}\{\|\mathbf{x}_m\|^2|U\} = \sum_{q \in \mathcal{Q}} \frac{P_{\max}}{Q} \|\mathbf{p}_{q,m}\|^2 \leq P_{\max}$, and therefore $\sum_{q \in \mathcal{Q}} \|\mathbf{p}_{q,m}\|^2 \leq Q, \forall m \in \mathcal{M}$. Because $\|\mathbf{p}_q\| = 1$, the latter constraint is always satisfied with strong inequality, implying that it is possible to increase the power. The objective of (S.9) is to guarantee that at least one S-RRH transmits with maximal power.²³ Considering the P&Q scheme, the strategy in Definition 8 applies with a minor modification. Each S-RRH serves exactly $Q - \bar{Q}$ MSs, with power $\tilde{P}_{q,m} = \tilde{P} = \frac{\tilde{\gamma} P_{\max}}{Q - \bar{Q}}, \forall q \in \mathcal{Q}, m \in \mathcal{M}$, where $\tilde{\gamma}$ is defined similarly to (S.9) while substituting $\tilde{\mathbf{p}}_{q,m}$ for $\mathbf{p}_{q,m}$ and $Q - \bar{Q}$ for Q .

Fig. 3(a) presents the throughput as a function of each S-RRH transmit power, P_{\max} (cf. Assumption 2). Fig. 3(b) presents the average throughput as a function of B , under a per-S-RRH power constraint of $P_{\max} = 45$ dBm.

²³Note that while this power allocation strategy is not optimal, it yields good performance in high SNRs.